

REVIEW ARTICLE | SEPTEMBER 06 2023

Molecular dynamics simulations of electrochemical interfaces

Liang Zeng ; Jiaxing Peng ; Jinkai Zhang ; Xi Tan ; Xiangyu Ji; Shiqi Li ; Guang Feng  



J. Chem. Phys. 159, 091001 (2023)
<https://doi.org/10.1063/5.0160729>



View
Online



CrossMark
Export
Citation

Articles You May Be Interested In

Experimental Investigation of Airbreathing Laser Propulsion Engines: CO₂TEA vs. EDL

AIP Conference Proceedings (April 2005)

Superionic liquids in conducting nanoslit: A variety of phase transitions and ensuing charging behavior

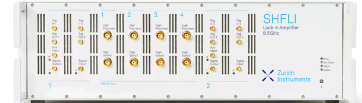
J. Chem. Phys. (November 2019)

Pulsed Laser Propulsion Performance of 11-cm Parabolic 'Bell' Engines: CO₂ TEA vs. EDL

AIP Conference Proceedings (May 2006)

500 kHz or 8.5 GHz?
And all the ranges in between.

Lock-in Amplifiers for your periodic signal measurements



Find out more

 Zurich
Instruments

Molecular dynamics simulations of electrochemical interfaces

Cite as: J. Chem. Phys. 159, 091001 (2023); doi: 10.1063/5.0160729

Submitted: 5 June 2023 • Accepted: 14 August 2023 •

Published Online: 6 September 2023



View Online



Export Citation



CrossMark

Liang Zeng,  Jiaxing Peng,  Jinkai Zhang,  Xi Tan,  Xiangyu Ji, Shiqi Li,  and Guang Feng^a 

AFFILIATIONS

State Key Laboratory of Coal Combustion, School of Energy and Power Engineering, Huazhong University of Science and Technology (HUST), Wuhan 430074, China

^aAuthor to whom correspondence should be addressed: gfeng@hust.edu.cn

ABSTRACT

Molecular dynamics (MD) simulations have become a powerful tool for investigating electrical double layers (EDLs), which play a crucial role in various electrochemical devices. In this Review, we provide a comprehensive overview of the techniques used in MD simulations for EDL studies, with a particular focus on methods for describing electrode polarization, and examine the principle behind these methods and their varying applicability. The applications of these approaches in supercapacitors, capacitive deionization, batteries, and electric double-layer transistors are explored, highlighting recent advancements and insights in each field. Finally, we emphasize the challenges and potential directions for future developments in MD simulations of EDLs, such as considering movable electrodes, improving electrode property representation, incorporating chemical reactions, and enhancing computational efficiency to deepen our understanding of complex electrochemical processes and contribute to the progress in the field involving EDLs.

Published under an exclusive license by AIP Publishing. <https://doi.org/10.1063/5.0160729>

I. INTRODUCTION

Electrical double layers (EDLs), solid–liquid interfaces between charged electrodes and electrolytes containing movable ions, are present in most electrochemical devices, such as batteries and supercapacitors, playing a crucial role in their performance.^{1–5} Modeling the EDL has become an important approach to understanding electrochemical phenomena, such as ionic structure, capacitance, and charging dynamics, further contributing to the design and optimization of these electrochemical devices.^{6–10}

In 1853, EDLs were initially defined by Helmholtz as two flat planar carrying equal but opposite charges, representing the charged electrodes and the counterions in the electrolyte.¹¹ Later, the Poisson–Boltzmann theory, developed by Gouy and Chapman, described the electrolyte side as an inhomogeneous ionic distribution in space.^{12,13} Stern further refined the theory by dividing the electrolyte into an inner layer (Stern layer) and a diffusion layer.¹⁴ Models based on Poisson–Boltzmann theory have been further developed to capture more physical properties, such as describing structural entropy by lattice gas models, thereby considering the effect of ion exclusion volumes.^{8,15,16} These theories provide valuable intuition for understanding a wide range of electrochemical phenomena and could serve as a guide for the optimization of

electrochemical devices. However, with the advancement of electrochemical systems and especially the application of nanomaterials, these theories may struggle to characterize factors including nanoconfinement by electrodes, non-dilute electrolytes, and high working voltages (far exceeds the thermal voltage).^{9,10} Hence, simulations at the atomistic level are urgently needed to provide a precise microscopic picture of EDLs.

First-principles calculations based on quantum mechanics can capture the electron distribution of electrodes and electrolytes in electrochemical systems.¹⁰ Although some empirical models have been developed to address solvation and electrode polarization, the computational costs remain high, limiting the scope to systems involving a small number of atoms (usually within 1000).^{10,17} In contrast, molecular dynamics (MD) simulations offer sufficient sampling for systems containing complex electrodes and electrolytes at a reasonable computational expense. With the development of methods to describe electrode polarization (i.e., how to describe the voltage/current applied to electrodes), MD has become a powerful tool for exploring the thermodynamic and kinetic behavior of EDLs.^{7,9,10}

In this Review, we aim to provide a comprehensive and up-to-date overview of the techniques used in classical MD simulations for EDL, with a particular focus on methods describing electrode

polarization. We discuss the rationale behind these methods and examine the applicability of each to specific simulation systems. We then delve into the application of these methods across various fields, including supercapacitors, capacitive deionization, batteries, and electric double-layer transistors, highlighting recent advancements and insights. Finally, we discuss the current challenges and identify potential directions for future development, providing referable conclusions and recommendations for researchers in different fields.

II. METHODOLOGY

Like conventional MD simulations, EDL modeling is based on interaction potential between atoms (i.e., force fields) to solve Newton's equations of motion and obtain the trajectories of all atoms in the simulated system.^{7,9,10} Force fields describing electrolyte interactions are generally well-established and can be categorized into all-atom, united-atom, and coarse-grained models^{18,19} or polarizable and non-polarizable types depending on their ability to self-regulate according to local electric fields.²⁰ Depending on research requirements, the electrode can be constructed as an ideal geometry (e.g., planar slab and slit pore) or near-realistic morphologies [e.g., conductive metal-organic frameworks (MOFs)], and the electrode atoms are usually set as immovable due to their negligible expansion and the computational cost. Non-electrostatic interactions between electrode and electrolyte atoms are well-established,

such as the widely used Lennard-Jones potentials.⁷ As a result, the key to MD simulation of EDL lies in describing the electrostatic interactions associated with the electrodes, specifically, the representation of electrode polarization. We briefly summarize the methods for describing electrode polarization, as shown in Fig. 1, ranging from the straightforward constant-charge method (CCM) to several approaches with the constant potential method (CPM) that can self-consistently respond to the applied voltage/current and the motion of solvent and ions in electrolytes.

A. Constant charge method

The most straightforward and computationally inexpensive approach is CCM, which uniformly and explicitly distributes the net charge of an electrode discretely over its atoms or smoothly over its surface, as illustrated by Fig. 1(a). It is noteworthy that whether the charge distribution is discrete or smooth CCM is shown to have a non-negligible effect on the structure of EDL and the differential capacitance.²¹ In some simulations for slab systems containing a pair of planar electrodes, the electrodes do not carry any charge, and the applied voltage is represented by a uniform electric field parallel to the normal of the electrodes,⁷ which is theoretically equivalent to a CCM with smooth surface charges.

The CCM is often adopted to study the equilibrium properties of systems with open electrodes (defined as an electrode whose

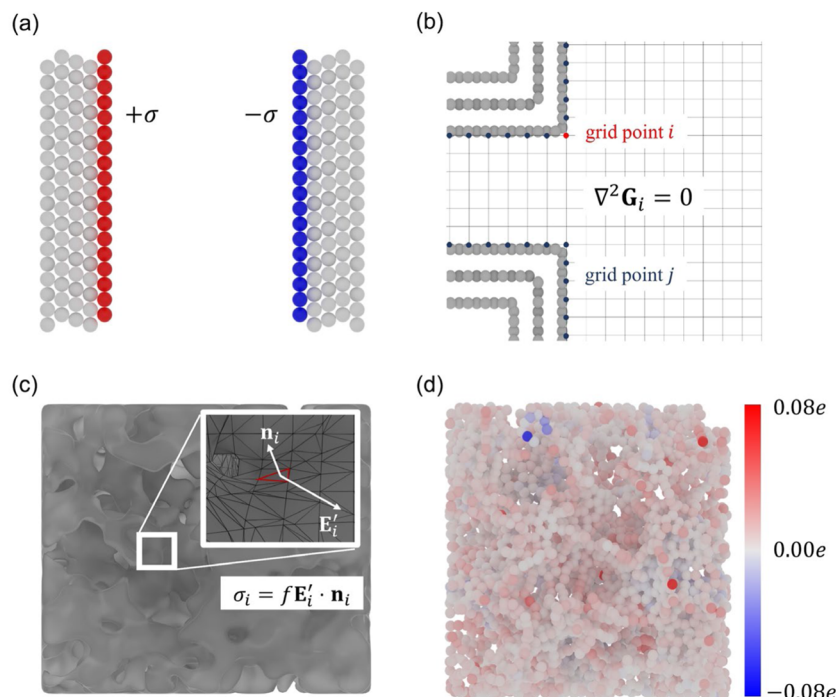


FIG. 1. Schematics describing the method of electrode polarization. (a) Constant charge method applies uniform charge densities $+\sigma$ ($-\sigma$) on flat electrode surfaces. (b) Green's function method shows an array for Green's function of single i th electrode grid points, the red point represents the boundary condition where $G = 1$ ($j = i$), and blue represents $G = 0$ ($j \neq i$), and the system is controlled by Laplace equation $\nabla^2 G_i = 0$. (c) ICC method calculates induced charge on surface elements on the dielectric boundary through the dot product of normal vector n_i and local electric field E'_i . (d) Fluctuating charge method allows the charge of electrode atoms to fluctuate in every time step to maintain electrode equipotential (atoms colored by their instantaneous charges).

surface is in contact with bulk electrolyte²²) that exhibit no confinement effects and can be reduced to one-dimensional structures, such as electrodes of graphene, carbon onions, and carbon nanotubes.^{23,24} In these simulations, electrolytes rearrange after applying electrode charges, and then, the information such as ionic structure can be obtained explicitly. However, the voltage between electrodes is not *a priori* and must be determined through post-processing based on Poisson's equation with the applied electrode charge and charge distribution of electrolytes, allowing further analysis of potential-related information, such as differential capacitance.²⁰ CCM can be extended to study dynamic charging and discharging processes in current mode by pre-setting the time-varying total charge on the electrode and uniformly distributing it among electrode atoms.²⁵ The galvanostatic charge–discharge (GCD) processes of supercapacitors with electrolyte as ionic liquid (IL) and electrodes as graphene plates,^{25,26} slit-nanopore,²⁵ and Mxenes^{27–29} were studied using this extended CCM.

The electrode atom charge in the CCM-based approach is pre-set and cannot dynamically respond to the movement of the electrolyte atoms, ignoring the fact that the electrode is equipotential. Hence, in principle, this approach is not accurate enough to describe the electrode polarization.^{20,25,30} In Secs. II B–II E, we introduce several methods describing electrode polarization that can ensure the equipotential state of electrodes and dynamically respond to changes in the electrolyte structure.

B. Green's function method

To make the electrodes equipotential in the MD system, the method of Green's function can be employed.^{31,32} In an electrochemical system with a charge density distribution of ρ_e , Poisson's equation $\nabla^2\phi = -\frac{\rho_e}{\epsilon_0}$ governs the distribution of electrical potential ϕ with boundary conditions $\phi = \phi^+$ and $\phi = \phi^-$, where $\phi^+(\phi^-)$ is pre-setting electrical potential of the positive (negative) electrode. In the Green's function method, ϕ can be divided into two parts as $\phi = \phi' + \phi_c$, where ϕ' is the potential that considers the explicit charge in the simulated system (i.e., charges from electrolytes) and ϕ_c is the potential from the boundary conditions, which are implicitly caused by the induced charge of the electrodes. Hence, Poisson's equation governing the electrical potential of the system can be divided into two parts as

$$\nabla^2\phi' = -\frac{\rho_e}{\epsilon_0}, \quad (1)$$

and

$$\nabla^2\phi_c = 0, \quad (2)$$

with boundary conditions of

$$\phi_c = \begin{cases} \phi^+ - \phi' & \text{for positive electrode,} \\ \phi^- - \phi' & \text{for negative electrode.} \end{cases} \quad (3)$$

For ϕ' in Eq. (1), classical electrostatic solution methods commonly used in MD, such as Ewald summation,³³ can be adopted to solve it.

The Laplace equation with boundary conditions presented in Eqs. (2) and (3) can be numerically solved using Green's function technique.³² In the technique, the discrete spatial array form of

Green's function \mathbf{G}^i is employed to calculate ϕ_c . \mathbf{G}^i is governed by $\nabla^2\mathbf{G}^i = 0$, with the boundary condition of

$$\mathbf{G}_j^i = \begin{cases} 1, & j = i, \\ 0, & j \neq i, \end{cases} \quad (4)$$

where i is a single electrode grid point where unit potential will be applied and j represents other electrode grid points, as illustrated by Fig. 1(b). According to the linearity of the Laplace equation, potential field ϕ_c can be solved as

$$\phi_c = \sum_i^{N_e} \mathbf{G}^i \phi_i, \quad (5)$$

where ϕ_i is the value of ϕ_c at the position of grid point i as given by Eq. (3) and N_e refers to the total number of electrode grids. The combination ϕ_c and ϕ' yields ϕ , which eventually provides the electrostatic force of all charged particles in the electrolyte.

C. ICC method

The equipotential electrodes can be described by the induced charge computation (ICC) method, which calculates the induced charge on polarized dielectric electrode–electrolyte boundaries, as illustrated in Fig. 1(c). These boundaries have varying permittivity at the interface between the electrode and electrolyte, and the electrical field controlled by the boundary conditions is³⁴

$$\epsilon_{out}\mathbf{E}^{out} \cdot \mathbf{n} = \epsilon_{in}\mathbf{E}^{in} \cdot \mathbf{n}, \quad (6)$$

$$(\mathbf{E}^{in} - \mathbf{E}^{out}) \cdot \mathbf{n} = \frac{4\pi\sigma}{\epsilon_{out}}, \quad (7)$$

where ϵ_{in} (ϵ_{out}) and \mathbf{E}^{in} (\mathbf{E}^{out}) are the local permittivity and electric field inside (outside) the electrode media. σ is the induced charge density on the boundary, and \mathbf{n} denotes the normal vector of the boundary surface. Equation (6) describes the continuity of polarization $\epsilon\mathbf{E}$ along the normal vector direction, while Eq. (7) elucidates the electric field mutation caused by induced charge σ .

To isolate the contribution of induced charge from \mathbf{E}^{in} and \mathbf{E}^{out} , the dielectric boundary is discretized into planar surface elements. For the surface element i , the induced charge will generate an electric field of $\frac{2\pi\sigma_i\mathbf{n}_i}{\epsilon_{out}}$, and thus,

$$\mathbf{E}_i^{in/out} = \mathbf{E}'_i \pm \frac{2\pi\sigma_i\mathbf{n}_i}{\epsilon_{out}}, \quad (8)$$

where \mathbf{E}'_i is the electric field caused by the charge from electrolytes and induced charges on other surface elements. By combining Eqs. (6) and (8), the induced charge of element i can be expressed as

$$\sigma_i = \frac{\epsilon_{out}}{2\pi} \left(\frac{\epsilon_{in} - \epsilon_{out}}{\epsilon_{in} + \epsilon_{out}} \right) \mathbf{E}'_i \cdot \mathbf{n}_i = f \mathbf{E}'_i \cdot \mathbf{n}_i, \quad (9)$$

where coefficient f is defined as $\frac{\epsilon_{out}}{2\pi} \left(\frac{\epsilon_{in} - \epsilon_{out}}{\epsilon_{in} + \epsilon_{out}} \right)$ to simplify the formula. Since \mathbf{E}'_i is dependent on the induced charges of other surface elements, the direct calculation of σ_i takes the linear algebraic form

of $\sum_j (\delta_{ij} - f K_{ij}) \sigma_j = f \mathbf{E}_i^{\text{electrolyte}} \cdot \mathbf{n}_i$, where δ_{ij} is Kronecker delta function. K_{ij} is the electrical response between induced charges from element i to element j , only depending on the position of the elements.³⁵ $\mathbf{E}_i^{\text{electrolyte}}$ is the electric field from electrolyte charges.

Furthermore, Tyagi *et al.*³⁴ developed an extension to this approach, known as ICC*. In this approach, Eq. (9) is solved by linear iteration as

$$\sigma_i^{(n+1)} = \omega(f \mathbf{E}'_i \cdot \mathbf{n}_i) + (1 - \omega)\sigma_i^{(n)}, \quad (10)$$

where ω is a relaxation coefficient determining the speed of convergence. At each iteration, σ_i is updated based on \mathbf{E}'_i , which is the external electric field calculated based on surface charges and electrolytes in the previous iteration. The charges that determine \mathbf{E}'_i are in explicit form, making this approach to allow for a scaleable and flexible algorithm that can accommodate different Coulomb solvers.

The ICC* method has undergone further development.^{36–38} The additional free charges, which exist in the absence of an electric field, are added to the induced charge in response to an external electric field [cf. Eq. (10)] as explicit charges at the electrode-electrolyte boundary.³⁶ The free charge is obtained based on an identical surface shape but with the medium replaced by a vacuum on the electrolyte side and a conductor on the electrode side.³⁶

To accelerate the computation of ICC*, various methods have been adopted for the calculation of induced charge. One such approach adopted is the generalized minimal residual method, which is commonly used to solve large and sparse linear systems, select the optimal approximation of surface charges in the Krylov space, and enable convergence in fewer steps.³⁶ Additionally, the pre-conditioning technique is employed to eliminate the ill-conditioned iteration matrix and improves the convergence of ICC*.³⁷ Another technique to speed up the ICC* is to use the fast multipole method as the Coulomb solver.³⁸ Notably, the fast multipole method offers significant advantages over $O(N \log N)$ approaches, such as Particle Mesh Ewald (PME) and Particle-Particle Particle-Mesh (PPPM) by reducing time complexity to $O(N)$ in extremely large systems.³⁸

D. Fluctuating charge method

We now discuss the method that allows the electrode atom charges to fluctuate at every time step, maintaining electrode equipotential, as illustrated by Fig. 1(d). Since the method was developed for simulating electrochemical cells by Reed *et al.*^{39,40} based on the work of Siepmann and Sprik,⁴¹ it has been further improved and advanced.^{25,42–51} Notably, this method has been integrated into software packages, such as MetalWalls,^{42,43} Large-scale Atomic/Molecular Massively Parallel Simulator (LAMMPS),^{47–50} and GROMACS,^{25,51} for a widespread application in electrochemistry.

In this method, the charges of electrode atoms typically take the form of Gaussian charges with a given width $\frac{1}{\eta}$ and fluctuating magnitude vector \mathbf{Q} . The charge distribution of atom i positioned at \mathbf{R}_i is expressed as

$$\rho_i(\mathbf{r}) = Q_i \left(\frac{\eta^2}{\pi} \right)^{\frac{3}{2}} \exp[-\eta^2(\mathbf{r} - \mathbf{R}_i)^2], \quad (11)$$

where Q_i is the element of \mathbf{Q} . The electrostatic energy U_{ele} of the system is a function of charge magnitude \mathbf{Q} and can be written in a quadratic form as

$$U_{ele}(\mathbf{Q}) = \frac{1}{2} \mathbf{Q}^T \mathbf{A} \mathbf{Q} - \mathbf{Q}^T \mathbf{B} + C. \quad (12)$$

In this equation, element A_{ij} in \mathbf{A} represents the electrostatic interaction coefficients describing the electrode atoms i and j , which depend on their positions. Element B_i in \mathbf{B} is the potential at the position of electrode atom i caused by the charge from electrolytes. C is the electrostatic energy only considering the charge from electrolytes. The calculation of \mathbf{A} and \mathbf{B} depends on whether the system is periodic in 2D or 3D, as described in Refs. 39, 43, and 52. The potential of electrode atom i is $\partial U_{ele} / \partial Q_i$, so the electrode equipotential conditions within an electrode are given by

$$\frac{\partial U_{ele}}{\partial Q_i} = \frac{\partial U_{ele}}{\partial Q_j} = \phi \quad \forall i, j, \quad (13)$$

where ϕ is the set potential for the electrode. To meet the equipotential constraint, \mathbf{Q} can be solved by a technique of extended Lagrangian dynamics^{53,54} or, more commonly, by minimizing U_T , which is given by

$$U_T = U_{ele} - \mathbf{Q}^T \phi. \quad (14)$$

This minimization can be performed by numerical iteration.^{43,52} However, in most simulated systems, electrode atoms are fixed, and a more efficient approach is to pre-solve the inverse of matrix \mathbf{A} before simulation and obtain electrode atom charges directly as

$$\mathbf{Q} = \mathbf{A}^{-1}(\mathbf{B} + \phi). \quad (15)$$

This is the fundamental principle of the approach, and based on this foundation, the approach has undergone further development. For instance, the above form pertains to cases where the electrode potentials are set, while the calculated \mathbf{Q} does not guarantee electrical neutrality in the system. For more practical scenarios, where the potential difference between the positive and negative electrodes is known and the system is electrically neutral, this can be achieved by modifying the matrix \mathbf{A} or adding Lagrangian constraints.^{49,53,55} For the calculation of the potential acting on the electrode atoms from the electrolyte (vector \mathbf{B}), the calculated speed can be improved by the meshed Ewald methods,^{56,57} implemented in widely used molecular dynamics software, such as GROMACS^{25,51} and LAMMPS.^{48,49} Simulation computation costs can also be reduced by employing a doubled-cell approach for systems with 2D periodicity.⁵⁰ The Gaussian distribution of electrode charge can be replaced by a point charge form with an energy term proportional to the square of the electrode charge as the electrostatic form of point charges is directly present in the majority of molecular dynamics codes.⁵⁸ When the force field describing the electrolyte is changed from non-polarized to polarized,²⁰ the variables to be solved encompass not only the electrode charge but also the induced dipole of the electrolyte, which has recently been implemented in the software of MetalWall.⁴³

In addition to explicitly setting the potential difference, the potential difference between electrodes can also be achieved by the finite electric field method with a constant potential electrode with

fluctuating charge.^{45,59} It should be noted that in the simulated system to which the method is applied, only one electrode is included (or rather two electrodes are next to each other) and the system is periodic in three dimensions, which saves computational costs.^{7,49} Similarly, by substituting the finite electric field with a finite electric displacement, this method can be extended to simulate the open-circuit state and the charging and discharging processes in the current control mode.⁴⁴ For the simulation of charging and discharging processes in current control mode, it can also be achieved by setting the electrode potentials to be solved and imposing constraints on the sum of electrode charges.²⁵ This method was applied to simulate galvanostatic charge–discharge processes for both planar and nanopore electrodes, capturing dynamics comparable to experimental results.²⁵

The discussion above has primarily focused on electrode atom charge fluctuations achieving pure electrostatic equipotentiality, considering electrodes as perfect conductors. However, this method can be easily extended to account for more quantum effects. One approach is to adjust the Gaussian width of the electrode charge to respond to the electrode's metallicity, which is operationally the simplest method and allows simulations to obtain capacitance values close to experimental ones.⁶⁰ Moreover, the energy determined by the fluctuating charge can include the band-structure energy from quantum calculations, thereby equilibrating the electrochemical potential of the electrode atoms. Then, the electrode charge is calculated by satisfying the constraint of equal electrochemical potential.⁶¹ The metallicity of the electrodes can also be considered using a semiclassical Thomas–Fermi theory, introducing the kinetic energy of electrons, where the degree of electrostatic screening of the electrodes can be described by the Thomas–Fermi length parameter.⁴⁶ Recently, the fluctuating charge method has been developed to consider the metallicity of electrodes containing multiple atom types, where different types of atoms have distinct Gaussian widths and pre-determined chemical potentials.⁶²

Aside from the aforementioned approaches with CPM, the approach with explicit image charges^{63–68} and the core–shell methods^{69–71} can also enable electrode polarization and take image charge effects into account. Nevertheless, these two methods are limited to simple electrode structures or are not easily applicable to potential differences. Furthermore, they have been discussed in existing literature,^{7,9,10} and thus, will not be elaborated on in this Review.

E. Which method should be selected?

The selection of methods for describing electrode polarization depends on various factors related to the system being simulated, such as the type of electrodes, electrolytes, voltage magnitude, and whether the simulation is in equilibrium or non-equilibrium. For CPM, methods based on image charges and core–shell are currently mainly applicable to systems with flat electrodes;^{63–71} the methods based on Green's function have been applied to systems containing flat electrodes and slit nanopore,^{31,32,72} while CPM based on ICC* and fluctuating charge can be applied to flat, slit nanopore, and even disorder porous materials.^{7,9} On the other hand, CCM only requires changing the charges of electrode atoms in the force field, which enables applied to any system technically, but this approach may lead to incorrect results.^{21,30,47,73–78}

CPM is more accurate and realistic than CCM,^{25,30,79} and it is also more complex to operate and requires significantly more computational resources. However, several studies have indicated that CCM can produce almost identical results to CPM in many systems.^{21,30,54,76} Therefore, determining the appropriate scenarios for employing the simpler and more cost-effective CCM, as well as situations must requiring CPM, is crucial to balance accuracy and computational efficiency.

The use of CCM for equilibrium simulations is influenced by factors such as electrode structure, electrolyte type, and voltage magnitude. For complex or nanoconfined electrodes, where electrode atom charges exhibit significant spatial inhomogeneity, the uniform charge application of CCM falls short when compared to CPM, rendering the latter indispensable.^{20,30,75} Therefore, CCM is generally more suitable for open electrode systems with ideal surfaces (e.g., graphene sheets, outer convex surfaces of carbon nanotubes, and carbon onions), although its applicability still depends on electrolyte type and voltage magnitude.

Simulations of systems containing ionic liquids (ILs) and flat electrodes have demonstrated that the consistency between CCM and CPM cannot be achieved at 9 V, a voltage far exceeding the electrochemical window of ILs.³⁰ However, within the electrochemical window range, CCM can achieve EDL structures nearly identical to those produced by CPM.^{21,30,54,76} It has been reported that minor structural differences between CCM and CPM in IL systems result in differential capacitance disparities,⁷³ possibly due to the structure's heightened sensitivity to differential capacitance. As a result, CCM can be employed to obtain equilibrium EDL structures for systems containing open electrodes and ILs. The feasibility of using CCM for aqueous electrolytes remains uncertain, as some research has shown little difference between CCM and CPM,¹⁰ while others report marked discrepancies in the EDL structures obtained by the two methods.⁷⁷ As for organic electrolytes, particularly those containing Li ions, CCM fails to capture accurate EDL structures,^{47,80} mainly because it neglects the pronounced image charge effect.^{47,80}

In non-equilibrium simulations of voltage-driven charging and discharging processes, CCM will produce overly rapid relaxation times and non-physical heat generation, which makes CPM indispensable.^{30,54} However, for current-driven processes, our recent findings indicate that a CCM-based approach can be applied to the galvanostatic charge–discharge process simulations for planar electrode systems containing ILs, yielding EDL structures and GCD curves nearly identical to those generated by CPM.²⁵

III. APPLICATIONS

Classical MD simulations combined with approaches describing electrode polarization can be applied to various fields involving EDLs. In this section, we will discuss the investigation of supercapacitors,^{1,81} capacitive deionization (CDI),⁸² batteries,^{4,83} and electrical double layer transistors (EDLTs),^{2,84} focusing on the key characteristics that can be obtained from MD simulations in these fields.

A. Supercapacitor

Supercapacitors, also known as electric double-layer capacitors, have emerged as an essential energy storage technology

due to their unique ability to combine high power density, rapid charge/discharge rates, and long cycle life.^{1,9,81,85} Central to the performance of supercapacitors are the EDLs formed at the interfaces between the electrodes and the electrolyte. The characteristics of the EDL, such as its structure, charge distribution, and ion dynamics, significantly impact the energy density, power density, and overall performance of supercapacitors.^{6,9} Therefore, understanding the fundamental mechanisms governing EDL behavior is crucial for optimizing supercapacitor performance and enabling broader adoption. MD simulations have emerged as a powerful tool for investigating the complex phenomena occurring within EDLs and providing valuable insights into the structural, dynamic, and electrochemical properties of supercapacitor systems.^{7,9,10,22}

1. Open electrode systems

In the majority of early simulations, supercapacitors were conceptualized as systems containing electrolytes and ideal open electrodes.^{3,86–91} From a technical standpoint, equilibrium simulations for these systems could be executed more cost-effectively using the CCM, as illustrated in Sec. II. The structures of EDLs and their relationships with capacitance have been extensively explored. These studies encompass a wide range of electrolytes, from aqueous^{32,92–94} and organic^{91,95} to ILs,^{8,86–90,96} and various electrode types, such as flat surfaces,^{72,97,98} convex carbon nanotube surfaces,^{24,99} and convex spherical surfaces of carbon onions.²³ By utilizing statistical analysis from simulations, one-dimensional density distributions for various components, along with charge and potential distributions, can be obtained to determine the (differential) capacitance, effectively bridging the gap between the microscopic structure of the EDL and its macroscopic performance. The significant finding of these simulations involves the layered EDL structures in ILs,^{8,86–90,96,99,100} which transition from “over-screening” to “crowding.”^{16,101} Consequently, the differential capacitance deviates from the classical Gouy–Chapman–Stern model^{12–14} and instead exhibits a “camel shape” or “bell shape,” as predicted by lattice gas mean-field theory.¹⁶ Moreover, the dependence of differential capacitance and EDL structures on the type of ILs and temperature has been examined,^{87,89,99,102} and the effects caused by curvature^{23,99} and roughness^{100,102} of electrodes have also been evaluated.

With the advanced understanding of “EDL life,”⁹² the analysis of EDL structures is more refined. In a plane parallel to the electrode, the adsorbed ions in ILs have been found to undergo structural transitions between ordered and disordered phases.^{92,103} These transitions are profoundly related to charge fluctuations on the electrode, differential capacitance, and hysteresis in the kinetic processes.^{92,104,105}

The refined description of the EDL structure was also represented in simulations exploring the impact of water impurities on the stability of ILs.^{72,97,98} It was revealed that even trace amounts of water present in the ILs could cause water to accumulate on the electrode surface, subsequently reducing the electrochemical window of the electrolyte.⁹⁷ This reduction can be mitigated by employing hydrophilic ILs⁷² or incorporating salt into ILs [as depicted in Fig. 2(a)].⁹⁸ In these studies, the location, orientation, hydrogen bonding, ion binding states, and infrared spectroscopy spectra of water molecules in the EDLs were meticulously characterized, with their voltage dependence also being comprehensively understood.

For instance, it was observed that the addition of salts led to a significant blue shift [increase in wavenumber, Fig. 2(b)] in the O–H bond vibration of water molecules.⁹⁸ This blue shift phenomenon increased the bond dissociation energy of the O–H bond, thereby decreasing water reactivity. Further analysis revealed that the blue shift phenomenon was caused by a reduction in water molecule clusters and the disruption of the hydrogen bond network as salts were added. This insight into the microscopic EDL structures of IL electrolytes containing trace amounts of water aids in understanding the macroscopic working voltage of these electrolytes. In conclusion, these studies emphasize that a more comprehensive understanding of EDL structures is necessary from both technical and mechanistic viewpoints, and it should not be confined to a one-dimensional description, even when the electrode has a smooth and flat surface.^{104,106}

2. Nanopore electrode systems

Following the experimental discovery of the anomalous increase in capacitance as pore size decreases,^{107–110} supercapacitor electrodes are primarily composed of nanoporous materials. To investigate the impact of nano-confinement, specifically the role of pore size on EDLs, electrodes are modeled as nanotubes¹¹¹ or slit pores^{112–114} in MD simulations. Simulations based on CPM with Green’s function have been employed to explore the capacitance of slit-shaped nanopores with IL and found that capacitance exhibits a U-shaped scaling curve behavior with pore widths ranging from 0.75 to 1.26 nm, in which the left branch of the capacitance scaling curve corresponds to the anomalous capacitance increase.¹¹³ Concurrently, other MD simulations revealed a more complex oscillatory behavior in capacitance-pore size relationships, with maximum capacitance values observed at both 0.7 nm and a larger pore size of 1.4 nm.¹¹² This oscillatory relationship was subsequently experimentally confirmed.¹¹⁵ The capacitance-pore size profile originates from changes in EDL structures under confinement, which can be explained as a superposition of EDLs on both electrode walls, analogous to wave interference. Vatamanu *et al.*¹¹⁴ further conducted simulations on several systems featuring various ILs and nanopore electrodes (slit pores, cylindrical pores, and slit pores with rough walls in different pore sizes) to investigate capacitance behaviors. They also observed the anomalous capacitance increase and found that electrode roughness enhances capacitance as well. A similar dependence of capacitance on pore size has also been investigated in aqueous and organic systems.^{116,117}

The dynamic processes of EDLs under confinement, relating to the power density of supercapacitors, have been extensively investigated by MD simulations with nanotubes and slit nanopores. Kondrat and colleagues used MD based on CPM with Green’s function to study the charging dynamics of slit pores.¹¹⁸ For ionophilic pores (ions wetted in the pores at a non-polarized state), the charging process is a diffusion process accelerated by the collective effect. Moreover, when the voltage is large or close to zero, the diffusion within the pores is slower than in the bulk electrolyte. When the voltage is at an intermediate level, the diffusion is an order of magnitude larger than that in the bulk electrolyte. Conversely, when the electrodes are ionophobic (ions cannot enter the pores at a non-polarized state), the charging process can be accelerated due to the absence of overfilling or de-filling caused by ion congestion at the beginning of charging. The dependence of charging dynamics on

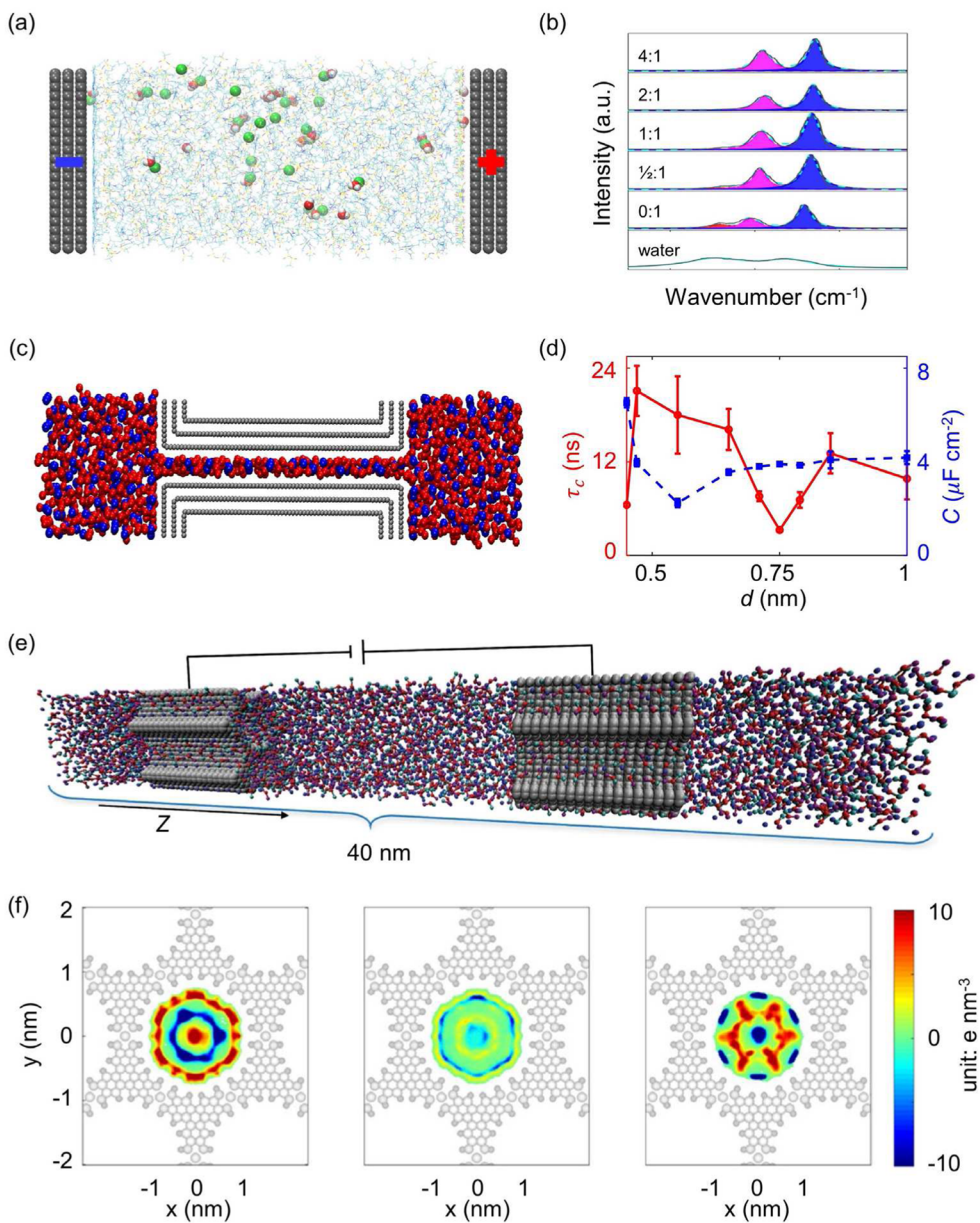


FIG. 2. Applications of MD simulations in the investigation of supercapacitors. (a) Simulation system featuring an open electrode model of graphene and a humid IL electrolyte with added salt. (b) Computed infrared spectroscopy (IR) spectra of O-H bonds in pure water, humid ILs, and humid ILs with varying salt-to-water molar ratios. The gray lines denote the IR spectra, while the red, pink, and blue regions correspond to the first, second, and third fitted spectra, respectively. The cyan dashed lines represent the sum of the fitted spectra. (a) and (b) are reproduced with permission from Chen *et al.*, Nat. Commun. **11**, 5809 (2020). Copyright 2020 Author(s), licensed under a Creative Commons Attribution (CC BY) license. (c) Simulation system featuring a slit nanopore electrode and an IL electrolyte. (d) Charging time constant (τ_c on the left y-axis) and capacitance (C on the right y-axis) as a function with pore size d . (c) and (d) are reproduced with permission from Mo *et al.*, ACS Nano **14**, 2395 (2020). Copyright 2020 American Chemical Society. (e) Simulation system featuring the realistic electrode models of $\text{Ni}_3(\text{HITP})_2$ MOF and $[\text{Emim}][\text{BF}_4]$ electrolyte. (f) Two-dimensional charge density from electrolyte along the pore axis inside the MOF pores. (e) and (f) are reproduced with permission from Bi *et al.*, Nat. Mater. **19**, 552 (2020). Copyright 2020 Springer Nature.

the pore size of slit nanopore electrodes has been investigated by MD simulations based on CPM with fluctuating charge [Fig. 2(c)].¹¹⁹ It was found that, contrary to the conventional understanding that larger pores lead to faster charging, the charging time oscillates as the pore size increases [Fig. 2(d)]. Charging is accelerated at specific pore sizes, and these pores can simultaneously achieve higher energy density and larger power density, which are determined by the transition structures of ions.

Most of the dynamic processes, including the works discussed above, are driven by voltages in a jump-wise mode (voltage steps from 0 to a value). However, Breitsprecher and colleagues used CPM-MD simulations based on ICC* to study the charging process of slit pores and found that, compared to jump-wise voltages, applying linear or nonlinear ramp voltages could avoid congestion caused by counter-ions at the beginning of charging, resulting in faster charging rates.^{120,121} This finding has been experimentally confirmed.¹²¹ Similar acceleration due to ramp voltage has been observed in simulations of carbon nanotube charging.¹²² For discharging, since there are no congestion issues, directly stepping the voltage down to 0 V or even applying a reverse voltage can result in faster discharging rates.^{120,121} In addition, the dynamic processes of ion transport in slit nanopores driven by periodic triangular wave voltages, or square wave currents set by the current-mode CPM, have been investigated, which helps understand the cyclic voltammetry and GCD test in electrochemical measurements.^{25,123}

3. Realistic electrode systems

To further explore energy storage mechanisms closer to real conditions, more complex MD simulation systems involving “realistic electrodes” should be employed. These account for the intricate structural and chemical properties of actual electrode materials. As discussed in Sec. II, employing CPM for conducting MD simulations with these electrode models is essential.

The most frequently adopted electrode material for supercapacitors is amorphous porous carbons.^{1,85} It is necessary to construct atomic structure models that can reflect the electrochemical features of these carbons before conducting MD simulations. Quenched molecular dynamics simulations were performed to generate a series of carbide-derived-carbon (CDC) models by tuning the thermal quench rate, which was compared with experimental pore size distributions, specific surface areas, and adsorption isotherms.¹²⁴ These generated CDC models with ILs composed of supercapacitors were investigated using CPM with fluctuating charge,^{125–130} which get an experimentally matched specific mass capacitance,¹²⁵ and demonstrated that a positive relationship exists between the local charge storage on the electrode and the degree of confinement.¹²⁶ The charging dynamics of these systems, driven by jump-wise voltages, were also explored.¹²⁷ It was found that the charging rate is dependent on the average pore size, with smaller pore sizes charging more slowly. The dynamic processes can be scaled up to a macroscopic level by fitting an equivalent resistor-capacitor circuit.¹²⁷ Subsequent simulations involving these CDC electrodes showed that the capacitance and resistance in the equivalent circuit can be obtained directly from equilibrium simulations, without the need for fitting through dynamic process simulations.¹²⁹ This multi-scale modeling opens the door for a quantitative comparison between molecular-scale simulations and macroscopic experiments.¹²⁹ In addition to using quenched MD, the atomic structure model of amorphous

carbon can also be constructed by adjusting the positions of the electrodes through Monte Carlo simulations to match *in situ* small-angle x-ray scattering experimental data.¹³¹ This constructed electrode model was adopted to investigate supercapacitors with an aqueous electrolyte and found the relation between the electrode’s atom charge and the degree of confinement similar to that found in ILs.¹²⁶

Materials with ordered structures, such as ordered carbons,¹³² MXenes,^{133,134} and MOFs,^{135,136} have shown potential as supercapacitor electrodes. The atomic models for these materials can be more easily obtained as their well-defined structures require less complex construction or modification compared to disordered materials. For ordered carbon materials, atomic structure models of zeolite-templated carbons^{137–139} and ordered mesoporous carbon¹⁴⁰ have been adopted by MD simulations to study the mechanisms of these materials as supercapacitor electrodes. In zeolite-templated carbons, the capacitance was found to have a strong correlation with charge compensation per carbon atom, rather than a significant association with the electrode pore size.¹³⁸ A smaller local surface curvature radius led to higher charge compensation per carbon atom and greater capacitance. However, charging rate was strongly correlated with pore size, with smaller sizes resulting in slower charging overall.¹³⁸ Subsequently, the role of surface functional groups on the electrode of zeolite templated carbon was further analyzed in simulations.¹³⁹

Bi and colleagues performed CPM with fluctuating charges to investigate the capacitance and charging dynamics of supercapacitors composed of two-dimensional conductive MOFs and ILs, as illustrated in the simulation system in Fig. 2(e).⁵¹ The differential capacitance was found to exhibit a bell-shaped and double-humped pattern concerning pore size, and the relationship with the EDL structure inside the pores was clarified [Fig. 2(f)]. Moreover, by using a transmission line model, the microscopic simulation results were scaled up to the macroscopic scale, which was confirmed by experimental electrochemical measurements.⁵¹ Two-dimensional layered materials, such as MXenes and molybdenum disulfide, have also been studied as electrodes using MD simulations.^{27–29,62,141} For these materials, it is important to pay attention to whether the distance between electrode layers changes with alterations in the charging state. The GCD processes of supercapacitors composed of MXenes and ILs have been simulated, and, unlike most simulations where electrodes are fixed, the electrode volume was found to vary with charging, which is related to ion transportation.^{27,28}

B. Capacitive deionization

Desalination is a promising solution to address freshwater scarcity, which can be categorized into pressure-driven, thermal, and electrokinetic desalination.³ Pressure-driven desalination uses pressure to force water through a membrane, separating it from ions,¹⁴² while thermal desalination relies on evaporation and condensation to separate water from ions.¹⁴³ Both methods are energy-intensive and not cost-effective for widespread application. Capacitive deionization (CDI), an emerging electrokinetic desalination technology, is a more cost-effective and energy-efficient water desalination process. CDI employs an electric field between a cathode and an anode to drive ions to the electrode, removing them from water

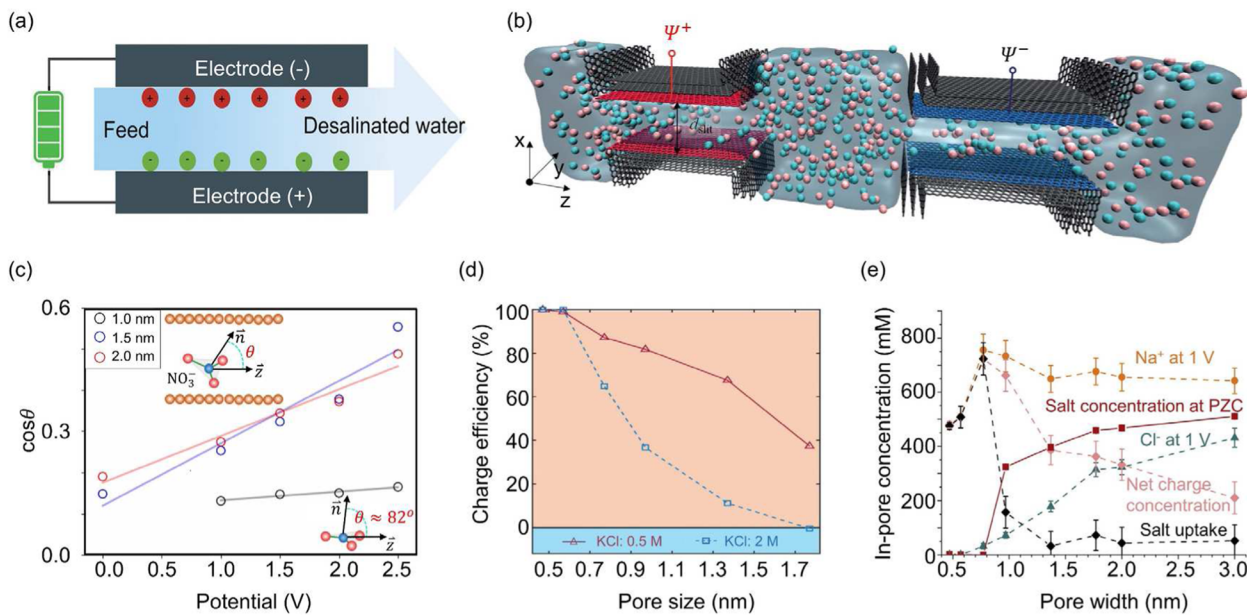


FIG. 3. Application of MD simulations in CDI systems. (a) Schematic of CDI. Reproduced with permission from Sun *et al.*, *Adv. Funct. Mater.* **33**, 2213578 (2023). Copyright 2023 John Wiley and Sons. (b) MD simulation system of slit pore applying potential for desalination. Reproduced with permission from Bi *et al.*, *Sustainable Energy Fuels* **4**, 1285 (2020). Copyright 2020 The Royal Society of Chemistry. (c) The angle between the NO_3^- normal and longitude direction of CNT at different voltages. Reproduced with permission from Mao *et al.*, *Chem. Eng. J.* **415**, 128920 (2021). Copyright 2021 Elsevier. (d) Charge efficiency of the CDI system as a function of pore size. Reproduced with permission from Bi *et al.*, *Sustainable Energy Fuels* **4**, 1285 (2020). Copyright 2020 The Royal Society of Chemistry. (e) Calculated in-pore ion uptake and release concentration, salt concentration at the potential of zero charge, net charge concentration, and salt uptake concentration. Reproduced with permission from Zhang *et al.*, *Cell Rep. Phys. Sci.* **3**, 100689 (2022). Copyright 2022 Author(s), licensed under a Creative Commons Attribution (CC BY) license.

[Fig. 3(a)].¹⁴⁴ MD simulations can elucidate the microscopic mechanism of desalination [Fig. 3(b)] and improve the performance of CDI systems.^{145–153}

1. Ion adsorption capacity

Salt removal capacity is the primary parameter determining the effectiveness of a CDI system. To investigate the effect of voltage application mode on the salt removal capacity in a CDI system, MD simulations with the CCM were conducted.¹⁴⁵ The simulations involved different CDI systems applying constant loading and pulse loading. The results indicate that the higher salt removal capacity of pulse loading is due to the intermittent load of the pulsed electric field. Using an appropriate load-unload frequency, the water dipole recovers from orientation polarization. In DC and extremely high-frequency voltage, the orientation polarization persists, preventing the electric field from driving ions to the electrode.

MD simulation is also used to explore the salt removal capacity of porous electrodes, such as carbon nanotubes (CNTs).^{146,147} Through MD simulations using CCM, it has been revealed that charged CNTs possess a hydrophilic nature, and water molecules penetrate ion pairs or clusters, which breaks the pair/cluster structure, making ion separation easier and eventually enhancing ion adsorption capacity and water purification. Moreover, the polarization of water molecules raises the dielectric constant and increases the availability of hydrogen bonding sites, making the dielectric

response faster.¹⁴⁸ This response significantly influences ion electrosorption capacity by affecting the Stern layer capacitance. Realistic electrode models are applied to investigate the ion adsorption capacity in amorphous porous carbons.¹⁴⁹ In this work, the pore size is comparable to the ion size, bringing the huge potential for deionization. The molecular simulation results at high concentrations can be used to parameterize a modified Donnan model, which can then be used to predict specific ion adsorption at lower concentrations.¹⁴⁹

2. Selectivity of ions

Nanoporous electrodes with selective ion adsorption capabilities can expand the potential applications of CDI. MD simulation studies indicate that pore geometry and applied voltage affect selectivity, which is determined by ion properties, including their charge and geometry.^{150,151} Simulations with CCM show that the best selectivity between Cl^- and NO_3^- occurs when the pore size is 2.0 nm for uncharged electrodes.¹⁵⁰ As voltage increases, the selectivity increases to a critical point before decreasing, with the maximum selectivity found at the critical point when the pore size is 1.5 nm. The mechanism of selectivity is examined from the perspective of molecular structure, such as hydrated radius and coordination number.¹⁵⁰ The planar structure of NO_3^- makes it easier to dehydrate and enter the pore, thus being more competitive for adsorption near the critical point. The voltage can adjust the angle between the NO_3^- plane normal vector and the longitudinal direction of the

CNT, thereby adjusting its entrance into the pore. Applying voltages to electrodes with 1.5 and 2.0 nm pores cause the normal of the NO_3^- plane and longitudinal direction to shift from being perpendicular to nearly parallel eventually [Fig. 3(c)]. This transition provides more strategies for NO_3^- to enter the pore, resulting in greater selectivity.¹⁵⁰

Besides the selectivity of anions, the selectivity of cations is also concerned and has been explored using MD simulations.¹⁵¹ The selectivity of Ca^{2+} over Na^+ and its dependence on the applied voltage in slit pores has been analyzed using CCM. The competition between ion-pore electrostatic interactions and crowding effects is considered to be the controlling factor of selectivity. At higher voltages, the dehydration shell of Ca^{2+} is more difficult to break, while the solvation shell of Na^+ is partially broken. As a consequence, Ca^{2+} demonstrates a larger volume and a decreased selectivity in comparison to Na^+ under these conditions.¹⁵¹

Beyond pore size, the shape of the electrode pores also significantly impacts ion transport processes,^{138,154,155} consequently playing a pivotal role in determining CDI selectivity. Through the application of density functional theory combined with a continuum solvation model, it has been observed that the cation binding energy in CNTs surpasses that in slit pores, especially for smaller ions, which makes CNTs more effective in separating Cs^+/Li^+ , Cs^+/Na^+ , and Cs^+/K^+ ions.¹⁵⁶ However, a more thorough comprehension of this area warrants further exploration through future MD simulations.

3. Permeability improves efficiency

The efficiency of CDI in removing high molar strength saline water is often lower than expected due to the simultaneous counterion adsorption and co-ion desorption processes in nanoporous electrodes.¹⁵⁷ MD simulations with CPM help address this problem by dynamically revealing underlying processes.^{152,153} It is found that in ionophobic pores (<0.6 nm), no ions are present inside the pore when not charged.¹⁵² When the potential is applied, only counter-ions are adsorbed, and no co-ion desorption occurs in these pores. The coordination number of water surrounding K^+ ions in these pores is smaller than that in ionophilic pores (>1.0 nm), indicating a fractured hydration shell. In such ionophobic pores, ions must overcome a higher dehydration energy barrier to enter the pore, which explains the absence of ions when the electrode is not charged. The initial state and dehydration process in ionophobic pores exhibit complete permeability of counter-ions, improving charge efficiency [Fig. 3(d)], and is consistent with experiments.¹⁵²

MD simulations using the CPM have revealed the permeability properties near the transition stage between ionophobic and ionophilic pores.¹⁵³ Ultra-micropores exhibit ionophobia, where the ion removal process only involves counter-ion adsorption without co-ion desorption, leading to high charge efficiency. However, the dehydration energy barrier increases significantly in ultra-micropores, reducing the absolute number of ion adsorption. To achieve the best desalination performance, a balance between the ionophobic nature and dehydration cost must be considered through the net charge concentration adsorbed by pores. The simulations have shown that the maximum net charge concentration and salt uptake concentration occur at a pore size of 0.77 nm [Fig. 3(e)], resulting in the best desalination performance.¹⁵³

C. Battery

The battery is the most widely used electrochemical energy storage device, providing the foundation for modern society by powering mobile devices and electric vehicles, serving as a crucial component in future energy storage facilities.⁵ The increasing demand for large-scale energy storage, driven by the development of renewable energy sources, necessitates higher battery performance, including high energy density, safety, temperature endurance, and long lifetime.¹⁵⁸ In a typical battery system, the interface between the electrode and electrolyte is the site of electron transfer, determining overall battery performance.¹⁵⁹ The in-depth understanding of interfaces within batteries remains a challenge due to their *in situ* nature and atomic-scale presence,¹⁶⁰ encouraging the application of *in situ* measurements¹⁶¹ and molecular simulations in battery research.⁴

Using MD simulations, the atomic EDL structure in the interfacial region under various potentials can be precisely depicted. Crucial characteristics of this structure, such as the orientation of interfacial water,⁹⁸ H-bond,^{162,163} and solvation structure,¹⁶⁴ significantly affect the interfacial reaction properties.¹⁶⁵ For instance, the orientation of interfacial water⁹⁸ and the connectivity of H-bond networks^{162,163} have been shown to influence electron transfer from the electrode to water and proton transfer in the interfacial region. Thus, gaining detailed information on interfacial structures helps unveil the mechanisms underlying interface regulation, thereby facilitating the design of batteries with improved performance.¹⁶⁶

1. Understanding the interfacial structure in batteries

Mixed carbon-based electrolytes, which may include dimethyl carbonate (DMC), ethylene carbonate (EC), or 1,3-dioxolane (DOL) as solvent, are commonly employed in commercial batteries.¹⁶⁷ Using ideal graphene sheets as electrodes, the interfacial structure of the EC:DMC(3:7)/LiPF₆ electrolyte (with a solvent to LiPF₆ molar ratio of about 2) under different potentials was simulated using CPM with fluctuating charge.¹⁶⁸ For both positively and negatively charged electrodes, EC with higher polarity, despite being the minority solvent, replaces DMC as polarization increases [Fig. 4(a)].¹⁶⁸ This is consistent with experimental observations of stronger adsorption of EC molecules on the LiCoO₂ cathode than linear carbonates.¹⁶⁹ Similarly, the interfacial structure of high concentration DMC/LiTFSI (with a solvent to LiPF₆ molar ratio of about 1.2) was simulated.¹⁷⁰ It was found that DMC is excluded from the positively charged electrode due to the distinct adsorption of the stable TFSI⁻ anion.¹⁷⁰ This restrains the side reaction of the solvent, explaining the suppression of current collector corrosion in high concentration.¹⁷¹

In addition to organic electrolytes, aqueous electrolytes are competitive candidates for future energy storage systems due to their intrinsic safety.¹⁷² In recent years, the high-concentrated “water-in-salt” electrolyte (WISE), with a wide electrochemical window, enables the realization of practical aqueous batteries.¹⁷³⁻¹⁷⁵ To understand the interfacial structure of WISE, Vatamanu and Borodin¹⁷⁶ conducted simulations of 28 m WISE comprising 21 m LiTFSI and 7 m LiOTF on polarized carbon electrodes using the CPM with fluctuating charge. It was revealed that TFSI⁻ anion shows stronger adsorption to the positively charged electrode than OTF⁻ anion. Simultaneously, water is largely excluded from the

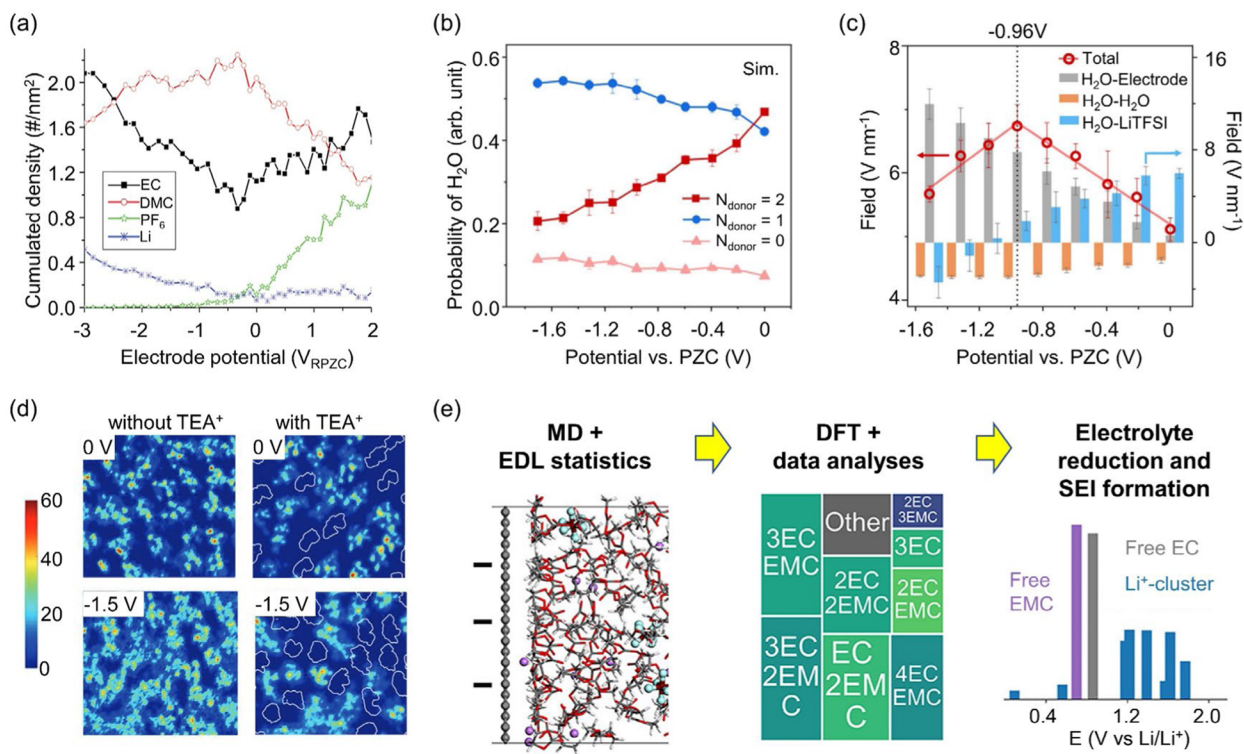


FIG. 4. Application of MD simulations in the investigation of batteries. (a) The interfacial density of electrolyte components of the EC:DMC(3:7)/LiPF₆ electrode under various potentials applied to carbon electrode. Reproduced with permission from Vatamanu *et al.*, J. Phys. Chem. C 116, 1114 (2012). Copyright 2012 American Chemical Society. (b) and (c) Simulated probability (b) and electric field strength (c) of interfacial water for 21 m LiTFSI on an Au(111) electrode. Reproduced with permission from Li *et al.*, Nat. Commun. 13, 5330 (2022). Copyright 2022 Author(s), licensed under a Creative Commons Attribution (CC BY) license. (d) The comparison of 2D density distributions of interfacial water at the anode before (left sub-graphs) and after (sub-graphs) adding TEA⁺ under 0 V (upper sub-graphs) and -1.5 V (upper bottom sub-graphs). The white lines sketch the contours of TEA⁺ distribution. The unit of the color bar is # nm⁻³. Reproduced with permission from Zhou *et al.*, Adv. Mater. 34, 2207040 (2022). Copyright 2023 John Wiley and Sons. (e) A scheme of the MD-DFT-data interactive model to investigate the effect of the EDL on electrolyte reduction and SEI formation. Reproduced with permission from Wu *et al.*, J. Am. Chem. Soc. 145, 2473 (2023). Copyright 2023 Author(s), licensed under a Creative Commons Attribution (CC BY) license.

electrode surface, explaining the improved oxidation stability of WISE.¹⁷⁶ By adding 21 m [MeEt₃N][TFSI], an extreme concentration of 63 m can be achieved.¹⁷⁷ As demonstrated by the MD simulations, the adsorbed water on the negatively charged electrode further decreases compared to 28 m WISE, achieving a wider electrochemical window.¹⁷⁷

The combination of *in situ* measurement and MD simulation can provide a more comprehensive and accurate depiction of the interfacial structure.^{79,170,178} By integrating shell-isolated nanoparticle-enhanced Raman spectroscopy (SHINERS) and MD simulations with CPM, an unconventional interfacial structure of 21 m LiTFSI at an Au(111) electrode was uncovered.⁷⁹ Simulations revealed that most of the interfacial water is bound by Li⁺, with different H-bond numbers ranging from 0 to 2 [Fig. 4(b)], in good agreement with three O-H stretching bands observed by SHINERS.⁷⁹ When polarization increases negatively, the adsorbed Li⁺ is inserted between the electrode and the first layer of water, weakening the electric field experienced by the water [Fig. 4(c)].⁷⁹ The trends in the electric field as a function of potential correspond well with vibrational frequency shifts in SHINERS. The adsorbed Li⁺ also leads to unusual “H-up” interfacial water molecules, with the

dipole pointing away from the electrode surface despite the negative electrode polarization.⁷⁹

2. Revealing the mechanisms of interface regulation to improve performance

Various strategies have been applied to regulate the interfacial structure for better battery performance. Using MD simulations, the mechanisms of interface regulation can be captured.^{165,179–182} For instance, in the case of a zinc-air battery, MD simulations based on CCM performed on the system with an ideal carbon electrode revealed that compared to SO₄²⁻, using OTF⁻ as the salt anion results in a reduced accumulation of water and increased presence of Zn²⁺ near the positively charged electrode, which suppresses the water-related oxygen reduction reaction and enhances reversibility.¹⁷⁹ Additionally, the interfacial structure can be effectively regulated by introducing additives. Using CCM to simulate the system with an ideal carbon electrode, Ma *et al.*¹⁶⁵ found that the addition of 4 m phosphonium cations effectively decreases the population of interfacial water. Zhou *et al.*¹⁸⁰ found that adding 1 m

TEA⁺ cation significantly improves the cathodic stability of a 13.8 m LiTFSI aqueous electrolyte with carbon-coated TiO₂. By conducting CPM simulations for a carbon electrode, the hydrophobic TEA⁺ is found to occupy more space on the electrode surface as the potential of electrode becomes more negative, blocking water from touching the electrode surface [Fig. 4(d)] and successfully suppressing the decomposition of water.¹⁸⁰

The introduction of NO₃⁻ anion has been proven to effectively improve the oxidation stability of ether-based electrolytes on cathodes.¹⁸³ Applying CCM on a carbon electrode, Zhang *et al.*¹⁸¹ found that the introduction of NO₃⁻ constructs a Li⁺-rich interface and forms unique polymer-like chain structures with high oxidation stability under positive potential. To consider the intrinsic charge of the cathode, Wang *et al.*¹⁸² coupled the atomic charge of the LiCoO₂ electrode from DFT calculation to the CPM-MD simulation, revealing that NO₃⁻ is dramatically absorbed on the electrode surface under positive potential, effectively expelling the solvent from the interfacial region and preventing solvent oxidation. However, an increase in bound solvent was not observed even though Li⁺ is accumulated with the introduction of NO₃⁻ in the interfacial region.¹⁸²

The decomposition of electrolytes during battery cycling leads to the formation of solid-electrolyte interphase (SEI), which prevents side reactions and improves battery reversibility.¹⁸⁴ MD simulations can help elucidate how the regulation of interfacial structure enhances SEI formation.^{181,185-187} For example, by conducting MD simulation on non-polarized Li metal, Huang *et al.*¹⁸⁵ compared the interfacial structure of electrolytes with various solvents, revealing that the solvent tris(trimethylsilyl) borate has the strongest adsorption on the electrode surface, promoting PF₆⁻ and Li⁺ in the interfacial region, and leading to the formation of an inorganic-rich SEI. Using CPM, Li₂DMC and Li₂TFSI aggregates were found near the negatively charged carbon electrode when DMC was introduced into the LiTFSI aqueous electrolyte, and these aggregates were more easily reduced to form SEI, as predicted by quantum chemistry calculation.¹⁸⁷ By conducting CPM simulations on a lithium anode, Wang *et al.*¹⁸⁸ found that due to strong anion-cation association, the introduced NO₃⁻ can accumulate near the electrode even under negative polarization, facilitating the formation of nitride-enriched SEI.

Simulating the systems with a graphene electrode by CCM, Wu *et al.*¹⁸⁹ explored the effect of fluoroethylene carbonate (FEC) on the interfacial structure of both carbonate and ether-based electrolytes. It is revealed that the Li-coordinated solvent is easier to be reduced on the negatively charged electrode than a free one.¹⁸⁹ To complement the electron transfer process missing in MD simulations, reduction potentials of representative structures were calculated by quantum chemistry calculation to understand SEI formation [Fig. 4(e)].¹⁸⁹ For the carbonate-based EC:EMC/LiPF₆ electrolyte, the SEI is derived from both free and cation-coordinated solvents but not anions. With the introduction of FEC, the density of F atoms in the interfacial region increases, promoting the LiF component in the SEI.¹⁸⁹ In contrast, for the ether-based DOL:DME/LiTFSI electrolyte, the SEI mainly originates from the Li⁺-coordinated solvents and anions, and the increase in F atoms due to FEC can only be observed at a low temperature of -40 °C,¹⁸⁹ which is consistent with experimental observations.¹⁹⁰

D. Electric double-layer transistor

The field-effect transistor is a critical component in modern semiconductor electronics. It comprises three terminals (source, gate, and drain) and controls the current flow by modulating the conductivity between the drain and source through changes in the gate-source voltage [Fig. 5(a)].^{2,191} Traditional field-effect transistors with inorganic solid-state materials as gate dielectrics suffer from limitations such as low capacitance and decreased carrier mobility.^{2,192,193} To overcome these issues, researchers have explored the use of EDLTs with liquid electrolytes instead. In EDLTs, the thickness of the EDL, which is only a few nanometers, results in high capacitance, leading to higher carrier accumulation, lower threshold voltage, and tunable electronic properties. Therefore, EDLTs have demonstrated promising performance and are considered a promising platform for next-generation electronic devices.^{2,84,194} The EDL between the channel and electrolyte is crucial in determining the performance of EDLTs, and using MD simulations to understand its microscopic characteristics is significant for understanding the working mechanism of EDLTs and optimizing their performance.¹⁹⁵⁻¹⁹⁹

1. Electrolyte structures

The effect of anion size on the interface structure in EDLTs with graphene and [Emim]⁺-based ILs has been investigated by MD simulations where electrodes are not polarized.¹⁹⁵ It was found that the imidazolium ring of the cation tends to be parallel to the graphene surface and build up a positive charge density, the extent of which becomes weaker as the anion size increases. Based on the structures, the positive shift in the Dirac point voltage observed by experiments is attributed to the induced negative charge density close to the graphene.

MD simulations based on CPM have explored the EDL structures varying with gate-source voltage in EDLTs consisting of amorphous indium gallium zinc oxide (a-IGZO) and ILs, which achieve excellent transistor performances with a relatively high current on/off ratio above 10⁷ and a threshold voltage less than 0.5 V.^{196,197} Simulations show that with the increase in the gate-source voltage, the number of cations in the first adsorption layer on the a-IGZO channel does not change significantly, while the orientation distribution of the imidazole ring dramatically changes as the imidazole ring is gradually distributed parallel to the channel surface [Fig. 5(b)].¹⁹⁶ This orientational change significantly reduces the thickness of the EDL and consequently increases the capacitance, which is in agreement with the measurement of the atomic force microscope.¹⁹⁶ The EDL structure transition shows a similar trend with the experimental conductivity of the a-IGZO channel, which exhibits a stepwise change with the gate-source voltage.¹⁹⁶

2. Distribution of charge carriers

In addition to investigating the EDL structures on the electrolyte side, MD simulations can also be used to explore the distribution of charge carriers on the solid side.¹⁹⁶⁻¹⁹⁸ In a study exploring the impact of ion size on the performance of EDLTs consisting of ILs and a-IGZO, MD simulations revealed that ILs with smaller ions can form a larger capacitance under the same gate-source voltage.¹⁹⁷ Subsequently, the influence of EDL microstructures on the uniformity of carrier distribution on the channel surface was

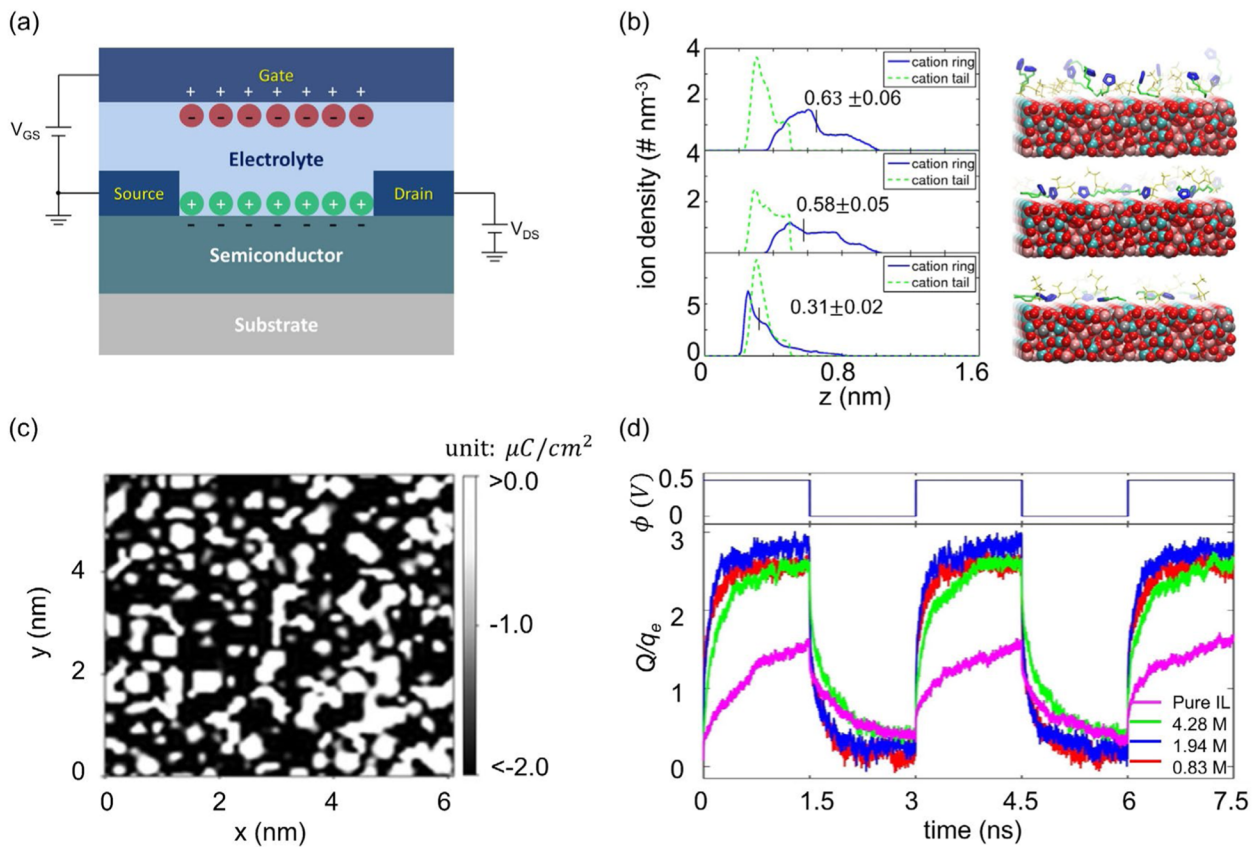


FIG. 5. Application of MD simulations in the investigation of EDLTs. (a) Schematic of EDLTs. Reproduced with permission from Du *et al.*, *J. Mater. Sci.* **50**, 5641 (2015). Copyright 2015 Springer Nature. (b) Structures of the first adsorbed cation on the a-IGZO surface, and the voltages from top to bottom are 0, 0.4, and 1.0 V. Reproduced with permission from Black *et al.*, *ACS Appl. Mater. Interfaces* **9**, 40949 (2017). Copyright 2017 American Chemical Society. (c) 2D distribution surface charge carrier density at the a-IGZO surface. Reproduced with permission from ACS Zhao *et al.*, *Appl. Mater. Interfaces* **10**, 43211 (2018). Copyright 2018 American Chemical Society. (d) Charging dynamics of MoS₂-based EDLTs for different concentrations of [Bmim][BF₄] in acetonitrile. The top panel of (d) shows that a pulsed square-shaped gate voltage was applied to the systems studied, and the bottom panel exhibits the time evolution of the total charge of the channel surface. q_e stands for the electric charge of an electron. Reproduced with permission from Zhao *et al.*, *ACS Appl. Mater. Interfaces* **11**, 13822 (2019). Copyright 2019 American Chemical Society.

analyzed [Fig. 5(c)]. It was found that smaller cations can induce a more uniform distribution of charge carriers. However, [BF₄]⁻, despite having the highest capacitance due to its small size, can induce the most non-uniform carrier distribution. Based on percolation theory analysis, it is concluded that the more uniform the carrier distribution, the higher the probability of forming conductive paths on the channel surface, potentially improving the conductivity.¹⁹⁷ A method based on resistance network analysis was further developed to quantitatively obtain the surface conductivity of the channel from the surface charge carrier distribution. The results confirmed that the more uniform the carrier distribution, the higher the conductivity of the channel. The simulation results were also magnified at the nanoscale to quantitatively compare with the experimental measurements at the macroscopic scale based on the conductivity of the channel, proving the reliability of this analysis method.¹⁹⁷

3. Dynamics

Besides the static characteristics of EDLTs, their dynamic properties, especially the switching speed,^{2,84,198} are also crucial and can

be studied using MD simulations.^{198,199} The dynamic performance of EDLTs mainly depends on the ion/molecule transport process in the EDLs, rather than the carrier mobility in the channel. To improve the dynamic performance of EDLTs with MoS₂, an organic solvent of acetonitrile was added to the IL [Bmim][BF₄] to enhance its diffusion performance, as investigated through MD simulations based on CPM.¹⁹⁸ From the amount of accumulated charge on the channel surface after applying the gate-source voltage, it was found that the addition of the organic solvent significantly improved the dynamic performance of the device [Fig. 5(d)]. Through the analysis of the electrolyte conductivity at different concentrations, it was found that the electrolyte concentration corresponding to the highest conductivity can achieve the optimal dynamic performance of the device. Therefore, the dynamic performance of the EDLT is mainly determined by the diffusion performance of the electrolyte. The addition of an organic solvent weakens the interaction between the adsorbed ions and the channel surface, resulting in a more uniform distribution of charge carriers and ultimately enhancing the channel's conductivity. Interestingly, the optimal

electrolyte concentration for achieving the most uniform carrier distribution on the channel surface was also the same as the one that optimized the dynamic performance of the EDLTs, which suggests that the addition of an organic solvent can simultaneously improve the static and dynamic performance of EDLTs.¹⁹⁸ Further simulations have shown that increasing the temperature can also enhance the dynamic performance of EDLTs, which is consistent with experimental findings.¹⁹⁹

IV. CONCLUSIONS AND PERSPECTIVES

MD simulation is a powerful tool for investigating EDLs at solid–liquid interfaces. Accurately modeling electrode polarization in these simulations remains a key challenge. We first provide an overview of several methods for describing electrode polarization in MD simulations, ranging from the straightforward CCM to more realistic CPM that maintains the equipotential of electrodes, including the approach with Green's function, ICC (ICC*), and the widely used method with fluctuating charges. We discuss the scenarios in which these approaches are applicable and, in particular, analyze the cases in which it may be possible to use the simpler and more computationally efficient CCM.

Finally, we present the application of MD in exploring several areas involving EDLs, including supercapacitors, CDI, batteries, and EDLTs. By utilizing different approaches and models for electrodes and electrolytes, MD simulations provide valuable insights into the structures and dynamics of EDLs and their mechanisms on system performance. These insights are crucial for optimizing system performance and expanding the potential applications of these technologies.

In the future of MD simulations of EDLs, it will be crucial to improve CPM techniques to capture more accurate EDL behaviors, providing valuable insights for the optimization of electrochemical devices. One key area of improvement is considering the metallic properties of electrodes as many electrodes are not perfect conductors.^{7,46,62} For example, the materials of channels in EDLT and quantum capacitance effects in the field of supercapacitors require a more accurate representation of electrode properties in simulations. Another important aspect is the incorporation of chemical reactions into MD simulations.^{200,201} The development and the use of reactive force fields in CPM-MD may help integrate these reactions into simulations, leading to a more comprehensive understanding of the processes and mechanisms involved in pseudocapacitive behavior and batteries. Moreover, introducing movable electrodes in simulations can enable the investigation of electrode expansion^{27,28} and heat conduction at the solid–liquid interface.^{202,203} Finally, enhancing computational efficiency is essential. Efforts to increase the scale of studied systems and improve simulation times are necessary. Leveraging the power of GPUs and combining machine learning techniques can help accelerate simulations and enable more efficient analysis.^{204,205}

Despite the promise and advancements in MD simulation techniques, it is crucial to recognize that these methods must be employed thoughtfully to avoid misleading results or the “garbage in, garbage out” phenomenon.²⁰⁶ In the pursuit of reliable and meaningful results, it is vital to adhere to best practices for simulations and calculations. This includes careful design of the system at the nanoscale, selecting the most appropriate method for the

study, utilizing state-of-the-art parameters and accuracy, and ensuring the collection of sufficient statistical data.²⁰⁶ By addressing these considerations and following these guidelines, the full potential of MD simulations for EDLs can be harnessed, leading to a deeper understanding of the complex electrochemical processes underlying electrochemical device performance and contributing to ongoing progress in the electrochemical field.

ACKNOWLEDGMENTS

The authors acknowledge the funding support from the National Natural Science Foundation of China (Grant Nos. T2325012, 52106090 and 52161135104) and the Program for HUST Academic Frontier Youth Team.

AUTHOR DECLARATIONS

Conflict of Interest

The authors have no conflicts to disclose.

Author Contributions

Liang Zeng: Writing – original draft (lead); Writing – review & editing (lead). **Jiaxing Peng:** Writing – original draft (supporting). **Jinkai Zhang:** Writing – original draft (supporting). **Xi Tan:** Writing – original draft (supporting). **Xiangyu Ji:** Writing – original draft (supporting). **Shiqi Li:** Writing – original draft (supporting). **Guang Feng:** Conceptualization (lead); Project administration (lead); Supervision (lead); Writing – review & editing (lead).

DATA AVAILABILITY

Data sharing is not applicable to this article as no new data were created or analyzed in this study.

REFERENCES

1. P. Simon and Y. Gogotsi, “Perspectives for electrochemical capacitors and related devices,” *Nat. Mater.* **19**(11), 1151–1163 (2020).
2. H. Chen, W. Zhang, M. Li, G. He, and X. Guo, “Interface engineering in organic field-effect transistors: Principles, applications, and perspectives,” *Chem. Rev.* **120**(5), 2879–2949 (2020).
3. K. Sun, M. Tebyetekerwa, C. Wang, X. Wang, X. Zhang, and X. S. Zhao, “Electrocapacitive deionization: Mechanisms, electrodes, and cell designs,” *Adv. Funct. Mater.* **33**(18), 2213578 (2023).
4. Y. Sun, T. Yang, H. Ji, J. Zhou, Z. Wang, T. Qian, and C. Yan, “Boosting the optimization of lithium metal batteries by molecular dynamics simulations: A perspective,” *Adv. Energy Mater.* **10**(41), 2002373 (2020).
5. J. Ma, Y. Li, N. S. Grundish, J. B. Goodenough, Y. Chen, L. Guo, Z. Peng, X. Qi, F. Yang, L. Qie, C.-A. Wang, B. Huang, Z. Huang, L. Chen, D. Su, G. Wang, X. Peng, Z. Chen, J. Yang, S. He, X. Zhang, H. Yu, C. Fu, M. Jiang, W. Deng, C.-F. Sun, Q. Pan, Y. Tang, X. Li, X. Ji, F. Wan, Z. Niu, F. Lian, C. Wang, G. G. Wallace, M. Fan, Q. Meng, S. Xin, Y.-G. Guo, and L.-J. Wan, “The 2021 battery technology roadmap,” *J. Phys. D: Appl. Phys.* **54**(18), 183001 (2021).
6. J. Wu, “Understanding the electric double-layer structure, capacitance, and charging dynamics,” *Chem. Rev.* **122**(12), 10821–10859 (2022).
7. L. Scalfi, M. Salanne, and B. Rotenberg, “Molecular simulation of electrode-solution interfaces,” *Annu. Rev. Phys. Chem.* **72**(1), 189–212 (2021).

- ⁸M. V. Fedorov and A. A. Kornyshev, "Ionic liquids at electrified interfaces," *Chem. Rev.* **114**(5), 2978–3036 (2014).
- ⁹G. Jeanmairet, B. Rotenberg, and M. Salanne, "Microscopic simulations of electrochemical double-layer capacitors," *Chem. Rev.* **122**(12), 10860–10898 (2022).
- ¹⁰R. Sundararaman, D. Vigil-Fowler, and K. Schwarz, "Improving the accuracy of atomistic simulations of the electrochemical interface," *Chem. Rev.* **122**(12), 10651–10674 (2022).
- ¹¹H. v. Helmholtz, "Ueber einige gesetze der vertheilung elektrischer ströme in körperlichen leitern, mit anwendung auf die thierisch-elektrischen versuche (schluss)," *Ann. Phys. Chem.* **165**(7), 353–377 (1853).
- ¹²M. Gouy, "Sur la constitution de la charge électrique à la surface d'un électrolyte," *J. Phys. Theor. Appl.* **9**(1), 457–468 (1910).
- ¹³D. L. Chapman, "LI. A contribution to the theory of electrocapillarity," *London, Edinburgh Dublin Philos. Mag. J. Sci.* **25**(148), 475–481 (1913).
- ¹⁴O. Stern, "Zur theorie der elektrolytischen doppelschicht," *Z. Elektrochem. Angew. Phys. Chem.* **30**(21–22), 508–516 (1924).
- ¹⁵I. Borukhov, D. Andelman, and H. Orland, "Steric effects in electrolytes: A modified Poisson-Boltzmann equation," *Phys. Rev. Lett.* **79**(3), 435–438 (1997).
- ¹⁶A. A. Kornyshev, "Double-layer in ionic liquids: Paradigm change?," *J. Phys. Chem. B* **111**(20), 5545–5557 (2007).
- ¹⁷R. Jinnouchi, K. Kodama, and Y. Morimoto, "Electronic structure calculations on electrolyte-electrode interfaces: Successes and limitations," *Curr. Opin. Electrochem.* **8**, 103–109 (2018).
- ¹⁸Y. Wang, W. Jiang, T. Yan, and G. A. Voth, "Understanding ionic liquids through atomistic and coarse-grained molecular dynamics simulations," *Acc. Chem. Res.* **40**(11), 1193–1199 (2007).
- ¹⁹J. Wang, S. Olsson, C. Wehmeyer, A. Pérez, N. E. Charron, G. de Fabritiis, F. Noé, and C. Clementi, "Machine learning of coarse-grained molecular dynamics force fields," *ACS Cent. Sci.* **5**(5), 755–767 (2019).
- ²⁰D. Bedrov, J.-P. Piquemal, O. Borodin, A. D. MacKerell, B. Roux, and C. Schröder, "Molecular dynamics simulations of ionic liquids and electrolytes using polarizable force fields," *Chem. Rev.* **119**(13), 7940–7995 (2019).
- ²¹K. Breitsprecher, K. Szuttor, and C. Holm, "Electrode models for ionic liquid-based capacitors," *J. Phys. Chem. C* **119**(39), 22445–22451 (2015).
- ²²J. Vatamanu, O. Borodin, M. Olguin, G. Yushin, and D. Bedrov, "Charge storage at the nanoscale: Understanding the trends from the molecular scale perspective," *J. Mater. Chem. A* **5**(40), 21049–21076 (2017).
- ²³G. Feng, D. Jiang, and P. T. Cummings, "Curvature effect on the capacitance of electric double layers at ionic liquid/onion-like carbon interfaces," *J. Chem. Theory Comput.* **8**(3), 1058–1063 (2012).
- ²⁴L. Yang, B. H. Fishbine, A. Migliori, and L. R. Pratt, "Molecular simulation of electric double-layer capacitors based on carbon nanotube forests," *J. Am. Chem. Soc.* **131**(34), 12373–12376 (2009).
- ²⁵L. Zeng, T. Wu, T. Ye, T. Mo, R. Qiao, and G. Feng, "Modeling galvanostatic charge-discharge of nanoporous supercapacitors," *Nat. Comput. Sci.* **1**(11), 725–731 (2021).
- ²⁶X. Jiang, J. Huang, H. Zhao, B. G. Sumpter, and R. Qiao, "Dynamics of electrical double layer formation in room-temperature ionic liquids under constant-current charging conditions," *J. Phys.: Condens. Matter* **26**(28), 284109 (2014).
- ²⁷K. Xu, C. Merlet, Z. F. Lin, H. Shao, P. L. Taberna, L. Miao, J. J. Jiang, J. X. Zhu, and P. Simon, "Effects of functional groups and anion size on the charging mechanisms in layered electrode materials," *Energy Storage Mater.* **33**, 460–469 (2020).
- ²⁸K. Xu, Z. Lin, C. Merlet, P.-L. Taberna, L. Miao, J. Jiang, and P. Simon, "Tracking ionic rearrangements and interpreting dynamic volumetric changes in two-dimensional metal carbide supercapacitors: A molecular dynamics simulation study," *ChemSusChem* **11**(12), 1892–1899 (2018).
- ²⁹K. Xu, X. Ji, B. Zhang, C. Chen, Y. Ruan, L. Miao, and J. Jiang, "Charging/discharging dynamics in two-dimensional titanium carbide (MXene) slit nanopore: Insights from molecular dynamic study," *Electrochim. Acta* **196**, 75–83 (2016).
- ³⁰C. Merlet, C. Pean, B. Rotenberg, P. A. Madden, P. Simon, and M. Salanne, "Simulating supercapacitors: Can we model electrodes as constant charge surfaces?," *J. Phys. Chem. Lett.* **4**(2), 264–268 (2013).
- ³¹A. V. Raghunathan and N. R. Aluru, "Self-consistent molecular dynamics formulation for electric-field-mediated electrolyte transport through nanochannels," *Phys. Rev. E* **76**(1), 011202 (2007).
- ³²C. Cagle, G. Feng, R. Qiao, J. Huang, B. G. Sumpter, and V. Meunier, "Structure and charging kinetics of electrical double layers at large electrode voltages," *Microfluid. Nanofluid.* **8**(5), 703–708 (2010).
- ³³P. P. Ewald, "Die berechnung optischer und elektrostatischer gitterpotentiale," *Ann. Phys.* **369**(3), 253–287 (1921).
- ³⁴S. Tyagi, M. Süzen, M. Segu, M. Barbosa, S. S. Kantorovich, and C. Holm, "An iterative, fast, linear-scaling method for computing induced charges on arbitrary dielectric boundaries," *J. Chem. Phys.* **132**(15), 154112 (2010).
- ³⁵D. Boda, D. Gillespie, W. Nonner, D. Henderson, and B. Eisenberg, "Computing induced charges in inhomogeneous dielectric media: Application in a Monte Carlo simulation of complex ionic systems," *Phys. Rev. E* **69**(4), 046702 (2004).
- ³⁶K. Barros, D. Sinkovits, and E. Luijten, "Efficient and accurate simulation of dynamic dielectric objects," *J. Chem. Phys.* **140**(6), 064903 (2014).
- ³⁷H. Wu and E. Luijten, "Accurate and efficient numerical simulation of dielectrically anisotropic particles," *J. Chem. Phys.* **149**(13), 134105 (2018).
- ³⁸X. K. Jiang, J. Y. Li, X. J. Zhao, J. Qin, D. Karpeev, J. Hernandez-Ortiz, J. J. de Pablo, and O. Heinonen, "An O(N) and parallel approach to integral problems by a kernel-independent fast multipole method: Application to polarization and magnetization of interacting particles," *J. Chem. Phys.* **145**(6), 064307 (2016).
- ³⁹S. K. Reed, O. J. Lanning, and P. A. Madden, "Electrochemical interface between an ionic liquid and a model metallic electrode," *J. Chem. Phys.* **126**(8), 084704 (2007).
- ⁴⁰S. K. Reed, P. A. Madden, and A. Papadopoulos, "Electrochemical charge transfer at a metallic electrode: A simulation study," *J. Chem. Phys.* **128**(12), 124701 (2008).
- ⁴¹J. I. Siepmann and M. Sprink, "Influence of surface topology and electrostatic potential on water/electrode systems," *J. Chem. Phys.* **102**(1), 511–524 (1995).
- ⁴²A. Marin-Laflèche, M. Haefele, L. Scalfi, A. Coretti, T. Dufils, G. Jeanmairet, S. K. Reed, A. Serva, R. Berthoin, C. Bacon, S. Bonella, B. Rotenberg, P. Madden, and M. Salanne, "MetalWalls: A classical molecular dynamics software dedicated to the simulation of electrochemical systems," *J. Open Source Softw.* **5**(53), 2373 (2020).
- ⁴³A. Coretti, C. Bacon, R. Berthoin, A. Serva, L. Scalfi, I. Chubak, K. Golovizina, M. Haefele, A. Marin-Laflèche, B. Rotenberg, S. Bonella, and M. Salanne, "MetalWalls: Simulating electrochemical interfaces between polarizable electrolytes and metallic electrodes," *J. Chem. Phys.* **157**, 184801 (2022).
- ⁴⁴T. Dufils, M. Sprink, and M. Salanne, "Computational amperometry of nanoscale capacitors in molecular simulations," *J. Phys. Chem. Lett.* **12**(18), 4357–4361 (2021).
- ⁴⁵T. Dufils, G. Jeanmairet, B. Rotenberg, M. Sprink, and M. Salanne, "Simulating electrochemical systems by combining the finite field method with a constant potential electrode," *Phys. Rev. Lett.* **123**(19), 195501 (2019).
- ⁴⁶L. Scalfi, T. Dufils, K. G. Reeves, B. Rotenberg, and M. Salanne, "A semiclassical thomas-fermi model to tune the metallicity of electrodes in molecular simulations," *J. Chem. Phys.* **153**(17), 174704 (2020).
- ⁴⁷Z. Wang, Y. Yang, D. L. Olmsted, M. Asta, and B. B. Laird, "Evaluation of the constant potential method in simulating electric double-layer capacitors," *J. Chem. Phys.* **141**(18), 184102 (2014).
- ⁴⁸L. J. V. Ahrens-Iwers and R. H. Meißner, "Constant potential simulations on a mesh," *J. Chem. Phys.* **155**(10), 104104 (2021).
- ⁴⁹L. J. V. Ahrens-Iwers, M. Janssen, S. R. Tee, and M. R. H. Electrode, "ELECTRODE: An electrochemistry package for atomistic simulations," *J. Chem. Phys.* **157**(8), 084801 (2022).
- ⁵⁰S. R. Tee and D. J. Searles, "Fully periodic, computationally efficient constant potential molecular dynamics simulations of ionic liquid supercapacitors," *J. Chem. Phys.* **156**(18), 184101 (2022).
- ⁵¹S. Bi, H. Banda, M. Chen, L. Niu, M. Chen, T. Wu, J. Wang, R. Wang, J. Feng, T. Chen, M. Dincă, A. A. Kornyshev, and G. Feng, "Molecular understanding of charge storage and charging dynamics in supercapacitors with MOF electrodes and ionic liquid electrolytes," *Nat. Mater.* **19**(5), 552–558 (2020).
- ⁵²T. R. Gingrich and M. Wilson, "On the Ewald summation of Gaussian charges for the simulation of metallic surfaces," *Chem. Phys. Lett.* **500**(1–3), 178–183 (2010).

- ⁵³A. Coretti, L. Scalfi, C. Bacon, B. Rotenberg, R. Vuilleumier, G. Ciccotti, M. Salanne, and S. Bonella, "Mass-zero constrained molecular dynamics for electrode charges in simulations of electrochemical systems," *J. Chem. Phys.* **152**(19), 194701 (2020).
- ⁵⁴T. Inagaki and M. Nagaoka, "Electrode polarization effects on interfacial kinetics of ionic liquid at graphite surface: An extended Lagrangian-based constant potential molecular dynamics simulation study," *J. Comput. Chem.* **40**(24), 2131–2145 (2019).
- ⁵⁵L. Scalfi, D. T. Limmer, A. Coretti, S. Bonella, P. A. Madden, M. Salanne, and B. Rotenberg, "Charge fluctuations from molecular simulations in the constant-potential ensemble," *Phys. Chem. Chem. Phys.* **22**(19), 10480–10489 (2020).
- ⁵⁶U. Essmann, L. Perera, M. L. Berkowitz, T. Darden, H. Lee, and L. G. Pederseen, "A smooth particle mesh Ewald method," *J. Chem. Phys.* **103**(19), 8577–8593 (1995).
- ⁵⁷E. L. Pollock and J. Glosli, "Comments on P³M, FMM, and the Ewald method for large periodic coulombic systems," *Comput. Phys. Commun.* **95**(2), 93–110 (1996).
- ⁵⁸J. Vatamanu, D. Bedrov, and O. Borodin, "On the application of constant electrode potential simulation techniques in atomistic modelling of electric double layers," *Mol. Simul.* **43**(10–11), 838–849 (2017).
- ⁵⁹C. Zhang and M. Sprik, "Finite field methods for the supercell modeling of charged insulator/electrolyte interfaces," *Phys. Rev. B* **94**(24), 245309 (2016).
- ⁶⁰A. Serva, L. Scalfi, B. Rotenberg, and M. Salanne, "Effect of the metallicity on the capacitance of gold–aqueous sodium chloride interfaces," *J. Chem. Phys.* **155**(4), 044703 (2021).
- ⁶¹L. Pastewka, T. T. Järvi, L. Mayrhofer, and M. Moseler, "Charge-transfer model for carbonaceous electrodes in polar environments," *Phys. Rev. B* **83**(16), 165418 (2011).
- ⁶²S. Bi and M. Salanne, "Co-ion desorption as the main charging mechanism in metallic 1T-MoS₂ supercapacitors," *ACS Nano* **16**, 18658 (2022).
- ⁶³S. Tyagi, A. Arnold, and C. Holm, "Electrostatic layer correction with image charges: A linear scaling method to treat slab 2D + h systems with dielectric interfaces," *J. Chem. Phys.* **129**(20), 204102 (2008).
- ⁶⁴E. Wernersson and R. Kjellander, "On the effect of image charges and ion-wall dispersion forces on electric double layer interactions," *J. Chem. Phys.* **125**(15), 154702 (2006).
- ⁶⁵K. A. Dwelle and A. P. Willard, "Constant potential, electrochemically active boundary conditions for electrochemical simulation," *J. Phys. Chem. C* **123**(39), 24095–24103 (2019).
- ⁶⁶A. P. dos Santos, M. Girotto, and Y. Levin, "Simulations of Coulomb systems with slab geometry using an efficient 3D Ewald summation method," *J. Chem. Phys.* **144**(14), 144103 (2016).
- ⁶⁷J. Hautman, J. W. Halley, and Y. J. Rhee, "Molecular dynamics simulation of water between two ideal classical metal walls," *J. Chem. Phys.* **91**(1), 467–472 (1989).
- ⁶⁸A. Calhoun and G. A. Voth, "Electron transfer across the electrode/electrolyte interface: Influence of redox ion mobility and counterions," *J. Phys. Chem.* **100**(25), 10746–10753 (1996).
- ⁶⁹I. L. Geda, H. Ramezani-Dakhel, T. Jamil, M. Sulpizi, and H. Heinz, "Insight into induced charges at metal surfaces and biointerfaces using a polarizable Lennard-Jones potential," *Nat. Commun.* **9**(1), 716 (2018).
- ⁷⁰F. Iori and S. Corni, "Including image charge effects in the molecular dynamics simulations of molecules on metal surfaces," *J. Comput. Chem.* **29**(10), 1656–1666 (2008).
- ⁷¹F. Iori, R. Di Felice, E. Molinari, and S. Corni, "GoLP: An atomistic force-field to describe the interaction of proteins with Au(111) surfaces in water," *J. Comput. Chem.* **30**(9), 1465–1476 (2009).
- ⁷²S. Bi, R. Wang, S. Liu, J. Yan, B. Mao, A. A. Kornyshev, and G. Feng, "Minimizing the electrosorption of water from humid ionic liquids on electrodes," *Nat. Commun.* **9**(1), 5222 (2018).
- ⁷³J. B. Haskins and J. W. Lawson, "Evaluation of molecular dynamics simulation methods for ionic liquid electric double layers," *J. Chem. Phys.* **144**(18), 184707 (2016).
- ⁷⁴S. W. Coles, M. Mishin, S. Perkin, M. V. Fedorov, and V. B. Ivaniščev, "The nanostructure of a lithium glyme solvate ionic liquid at electrified interfaces," *Phys. Chem. Chem. Phys.* **19**(18), 11004–11010 (2017).
- ⁷⁵J. Y. Yang, Z. Bo, H. C. Yang, H. L. Qi, J. Kong, J. H. Yan, and K. F. Cen, "Reliability of constant charge method for molecular dynamics simulations on EDLCs in nanometer and sub-nanometer spaces," *ChemElectroChem* **4**(10), 2486–2493 (2017).
- ⁷⁶S. Ntim and M. Sulpizi, "Role of image charges in ionic liquid confined between metallic interfaces," *Phys. Chem. Chem. Phys.* **22**(19), 10786–10791 (2020).
- ⁷⁷C. Y. Son and Z.-G. Wang, "Image-charge effects on ion adsorption near aqueous interfaces," *Proc. Nat. Acad. Sci.* **118**(19), e2020615118 (2021).
- ⁷⁸J. Gäding, G. Tocci, M. Busch, P. Huber, and R. H. Meißner, "Impact of confinement and polarizability on dynamics of ionic liquids," *J. Chem. Phys.* **156**(6), 064703 (2022).
- ⁷⁹C.-Y. Li, M. Chen, S. Liu, X. Lu, J. Meng, J. Yan, H. D. Abruña, G. Feng, and T. Lian, "Unconventional interfacial water structure of highly concentrated aqueous electrolytes at negative electrode polarizations," *Nat. Commun.* **13**(1), 5330 (2022).
- ⁸⁰S. W. Coles and V. B. Ivaniščev, "Simulation of a solvate ionic liquid at a polarizable electrode with a constant potential," *J. Phys. Chem. C* **123**(7), 3935–3943 (2019).
- ⁸¹M. Salanne, B. Rotenberg, K. Naoi, K. Kaneko, P. L. Taberna, C. P. Grey, B. Dunn, and P. Simon, "Efficient storage mechanisms for building better supercapacitors," *Nat. Energy* **1**(6), 16070 (2016).
- ⁸²P. Srimuk, X. Su, J. Yoon, D. Aurbach, and V. Presser, "Charge-transfer materials for electrochemical water desalination, ion separation and the recovery of elements," *Nat. Rev. Mater.* **5**(7), 517–538 (2020).
- ⁸³J. Chen, X. Fan, Q. Li, H. Yang, M. R. Khoshi, Y. Xu, S. Hwang, L. Chen, X. Ji, C. Yang, H. He, C. Wang, E. Garfunkel, D. Su, O. Borodin, and C. Wang, "Electrolyte design for LiF-rich solid–electrolyte interfaces to enable high-performance micro-sized alloy anodes for batteries," *Nat. Energy* **5**(5), 386–397 (2020).
- ⁸⁴T. Fujimoto and K. Awaga, "Electric-double-layer field-effect transistors with ionic liquids," *Phys. Chem. Chem. Phys.* **15**(23), 8983–9006 (2013).
- ⁸⁵P. Simon and Y. Gogotsi, "Materials for electrochemical capacitors," *Nat. Mater.* **7**(11), 845–854 (2008).
- ⁸⁶M. V. Fedorov and A. A. Kornyshev, "Ionic liquid near a charged wall: Structure and capacitance of electrical double layer," *J. Phys. Chem. B* **112**(38), 11868–11872 (2008).
- ⁸⁷J. Vatamanu, O. Borodin, and G. D. Smith, "Molecular insights into the potential and temperature dependences of the differential capacitance of a room-temperature ionic liquid at graphite electrodes," *J. Am. Chem. Soc.* **132**(42), 14825–14833 (2010).
- ⁸⁸G. Feng, J. S. Zhang, and R. Qiao, "Microstructure and capacitance of the electrical double layers at the interface of ionic liquids and planar electrodes," *J. Phys. Chem. C* **113**(11), 4549–4559 (2009).
- ⁸⁹M. Chen, Z. A. H. Goodwin, G. Feng, and A. A. Kornyshev, "On the temperature dependence of the double layer capacitance of ionic liquids," *J. Electroanal. Chem.* **819**, 347–358 (2018).
- ⁹⁰M. V. Fedorov and A. A. Kornyshev, "Towards understanding the structure and capacitance of electrical double layer in ionic liquids," *Electrochim. Acta* **53**(23), 6835–6840 (2008).
- ⁹¹G. Feng, J. Huang, B. G. Sumpter, V. Meunier, and R. Qiao, "Structure and dynamics of electrical double layers in organic electrolytes," *Phys. Chem. Chem. Phys.* **12**(20), 5468–5479 (2010).
- ⁹²C. Merlet, D. T. Limmer, M. Salanne, R. van Roij, P. A. Madden, D. Chandler, and B. Rotenberg, "The electric double layer has a life of its own," *J. Phys. Chem. C* **118**(32), 18291–18298 (2014).
- ⁹³P. S. Crozier, R. L. Rowley, and D. Henderson, "Molecular-dynamics simulations of ion size effects on the fluid structure of aqueous electrolyte systems between charged model electrodes," *J. Chem. Phys.* **114**(17), 7513–7517 (2001).
- ⁹⁴H. Yang, J. Yang, Z. Bo, X. Chen, X. Shuai, J. Kong, J. Yan, and K. Cen, "Kinetic-dominated charging mechanism within representative aqueous electrolyte-based electric double-layer capacitors," *J. Phys. Chem. Lett.* **8**(15), 3703–3710 (2017).
- ⁹⁵C. Merlet, M. Salanne, B. Rotenberg, and P. A. Madden, "Influence of solvation on the structural and capacitive properties of electrical double layer capacitors," *Electrochim. Acta* **101**, 262–271 (2013).
- ⁹⁶G. Feng, J. Huang, B. G. Sumpter, V. Meunier, and R. Qiao, "A "counter-charge layer in generalized solvents" framework for electrical double layers in neat and

- hybrid ionic liquid electrolytes," *Phys. Chem. Chem. Phys.* **13**(32), 14723–14734 (2011).
- ⁹⁷G. Feng, X. Jiang, R. Qiao, and A. A. Kornyshev, "Water in ionic liquids at electrified interfaces: The anatomy of electrosorption," *ACS Nano* **8**(11), 11685–11694 (2014).
- ⁹⁸M. Chen, J. Wu, T. Ye, J. Ye, C. Zhao, S. Bi, J. Yan, B. Mao, and G. Feng, "Adding salt to expand voltage window of humid ionic liquids," *Nat. Commun.* **11**(1), 5809 (2020).
- ⁹⁹G. Feng, S. Li, J. S. Atchison, V. Presser, and P. T. Cummings, "Molecular insights into carbon nanotube supercapacitors: Capacitance independent of voltage and temperature," *J. Phys. Chem. C* **117**(18), 9178–9186 (2013).
- ¹⁰⁰J. Vatamanu, O. Borodin, D. Bedrov, and G. D. Smith, "Molecular dynamics simulation study of the interfacial structure and differential capacitance of alkylimidazolium bis(trifluoromethanesulfonyl)imide [C_nmim] [TFSI] ionic liquids at graphite electrodes," *J. Phys. Chem. C* **116**(14), 7940–7951 (2012).
- ¹⁰¹M. Z. Bazant, B. D. Storey, and A. A. Kornyshev, "Double layer in ionic liquids: Overscreening versus crowding," *Phys. Rev. Lett.* **106**(4), 046102 (2011).
- ¹⁰²J. Vatamanu, L. Xing, W. Li, and D. Bedrov, "Influence of temperature on the capacitance of ionic liquid electrolytes on charged surfaces," *Phys. Chem. Chem. Phys.* **16**(11), 5174–5182 (2014).
- ¹⁰³S. A. Kislenko, I. S. Samoylov, and R. H. Amirov, "Molecular dynamics simulation of the electrochemical interface between a graphite surface and the ionic liquid [BMIM][PF₆]," *Phys. Chem. Chem. Phys.* **11**(27), 5584–5590 (2009).
- ¹⁰⁴B. Rotenberg and M. Salanne, "Structural transitions at ionic liquid interfaces," *J. Phys. Chem. Lett.* **6**(24), 4978–4985 (2015).
- ¹⁰⁵I. V. Voroshylova, H. Ers, B. Docampo-Álvarez, P. Pikma, V. B. Ivaniščev, and M. N. D. S. Cordeiro, "Hysteresis in the MD simulations of differential capacitance at the ionic liquid–Au interface," *J. Phys. Chem. Lett.* **11**(24), 10408–10413 (2020).
- ¹⁰⁶A. A. Kornyshev and R. Qiao, "Three-dimensional double layers," *J. Phys. Chem. C* **118**(32), 18285–18290 (2014).
- ¹⁰⁷J. Chmiola, G. Yushin, Y. Gogotsi, C. Portet, P. Simon, and P. L. Taberna, "Anomalous increase in carbon capacitance at pore sizes less than 1 nanometer," *Science* **313**(5794), 1760–1763 (2006).
- ¹⁰⁸N. Jäckel, P. Simon, Y. Gogotsi, and V. Presser, "Increase in capacitance by subnanometer pores in carbon," *ACS Energy Lett.* **1**(6), 1262–1265 (2016).
- ¹⁰⁹C. Largeot, C. Portet, J. Chmiola, P.-L. Taberna, Y. Gogotsi, and P. Simon, "Relation between the ion size and pore size for an electric double-layer capacitor," *J. Am. Chem. Soc.* **130**(9), 2730–2731 (2008).
- ¹¹⁰E. Raymundo-Piñero, K. Kierzek, J. Machnikowski, and F. Béguin, "Relationship between the nanoporous texture of activated carbons and their capacitance properties in different electrolytes," *Carbon* **44**(12), 2498–2507 (2006).
- ¹¹¹Y. Shim and H. J. Kim, "Nanoporous carbon supercapacitors in an ionic liquid: A computer simulation study," *ACS Nano* **4**(4), 2345–2355 (2010).
- ¹¹²G. Feng and P. T. Cummings, "Supercapacitor capacitance exhibits oscillatory behavior as a function of nanopore size," *J. Phys. Chem. Lett.* **2**(22), 2859–2864 (2011).
- ¹¹³P. Wu, J. Huang, V. Meunier, B. G. Sumpter, and R. Qiao, "Complex capacitance scaling in ionic liquids-filled nanopores," *ACS Nano* **5**(11), 9044–9051 (2011).
- ¹¹⁴J. Vatamanu, M. Vatamanu, and D. Bedrov, "Non-Faradaic energy storage by room temperature ionic liquids in nanoporous electrodes," *ACS Nano* **9**(6), 5999–6017 (2015).
- ¹¹⁵X. Wang, H. Zhou, E. Sheridan, J. C. Walmsley, D. Ren, and D. Chen, "Geometrically confined favourable ion packing for high gravimetric capacitance in carbon–ionic liquid supercapacitors," *Energy Environ. Sci.* **9**(1), 232–239 (2016).
- ¹¹⁶S. Bi, Z. Li, D. Xiao, Z. Li, T. Mo, G. Feng, and X. Zhang, "Pore-size-dependent capacitance and charging dynamics of nanoporous carbons in aqueous electrolytes," *J. Phys. Chem. C* **126**, 6854 (2022).
- ¹¹⁷K. Ma, X. Wang, J. Forsman, and C. E. Woodward, "Molecular dynamic simulations of ionic liquid's structural variations from three to one layers inside a series of slit and cylindrical nanopores," *J. Phys. Chem. C* **121**(25), 13539–13548 (2017).
- ¹¹⁸S. Kondrat, P. Wu, R. Qiao, and A. A. Kornyshev, "Accelerating charging dynamics in subnanometre pores," *Nat. Mater.* **13**(4), 387–393 (2014).
- ¹¹⁹T. Mo, S. Bi, Y. Zhang, V. Presser, X. Wang, Y. Gogotsi, and G. Feng, "Ion structure transition enhances charging dynamics in subnanometer pores," *ACS Nano* **14**(2), 2395–2403 (2020).
- ¹²⁰K. Breitsprecher, C. Holm, and S. Kondrat, "Charge me slowly, I am in a hurry: Optimizing charge-discharge cycles in nanoporous supercapacitors," *ACS Nano* **12**(10), 9733–9741 (2018).
- ¹²¹K. Breitsprecher, M. Janssen, P. Srimuk, B. L. Mehdi, V. Presser, C. Holm, and S. Kondrat, "How to speed up ion transport in nanopores," *Nat. Commun.* **11**(1), 6085 (2020).
- ¹²²A. J. Pak and G. S. Hwang, "Charging rate dependence of ion migration and stagnation in ionic-liquid-filled carbon nanopores," *J. Phys. Chem. C* **120**(43), 24560–24567 (2016).
- ¹²³Y. D. He, J. S. Huang, B. G. Sumpter, A. A. Kornyshev, and R. Qiao, "Dynamic charge storage in ionic liquids-filled nanopores: Insight from a computational cyclic voltammetry study," *J. Phys. Chem. Lett.* **6**(1), 22–30 (2015).
- ¹²⁴J. C. Palmer, A. Llobet, S. H. Yeon, J. E. Fischer, Y. Shi, Y. Gogotsi, and K. E. Gubbins, "Modeling the structural evolution of carbide-derived carbons using quenched molecular dynamics," *Carbon* **48**(4), 1116–1123 (2010).
- ¹²⁵C. Merlet, B. Rotenberg, P. A. Madden, P. L. Taberna, P. Simon, Y. Gogotsi, and M. Salanne, "On the molecular origin of supercapacitance in nanoporous carbon electrodes," *Nat. Mater.* **11**(4), 306–310 (2012).
- ¹²⁶C. Merlet, C. Péan, B. Rotenberg, P. A. Madden, B. Daffos, P. L. Taberna, P. Simon, and M. Salanne, "Highly confined ions store charge more efficiently in supercapacitors," *Nat. Commun.* **4**, 2701 (2013).
- ¹²⁷C. Pean, C. Merlet, B. Rotenberg, P. A. Madden, P. L. Taberna, B. Daffos, M. Salanne, and P. Simon, "On the dynamics of charging in nanoporous carbon-based supercapacitors," *ACS Nano* **8**(2), 1576–1583 (2014).
- ¹²⁸T. Méndez-Morales, N. Ganfoud, Z. Li, M. Haefele, B. Rotenberg, and M. Salanne, "Performance of microporous carbon electrodes for supercapacitors: Comparing graphene with disordered materials," *Energy Storage Mater.* **17**, 88–92 (2019).
- ¹²⁹C. Pean, B. Rotenberg, P. Simon, and M. Salanne, "Multi-scale modelling of supercapacitors: From molecular simulations to a transmission line model," *J. Power Sources* **326**, 680–685 (2016).
- ¹³⁰C. Pean, B. Daffos, C. Merlet, B. Rotenberg, P. L. Taberna, P. Simon, and M. Salanne, "Single electrode capacitances of porous carbons in neat ionic liquid electrolyte at 100 °C: A combined experimental and modeling approach," *J. Electrochem. Soc.* **162**(5), A5091–A5095 (2015).
- ¹³¹C. Prehal, C. Koczwara, N. Jäckel, A. Schreiber, M. Burian, H. Amenitsch, M. A. Hartmann, V. Presser, and O. Paris, "Quantification of ion confinement and desolvation in nanoporous carbon supercapacitors with modelling and *in situ* X-ray scattering," *Nat. Energy* **2**, 16215 (2017).
- ¹³²L. L. Zhang and X. S. Zhao, "Carbon-based materials as supercapacitor electrodes," *Chem. Soc. Rev.* **38**(9), 2520–2531 (2009).
- ¹³³M. R. Lukatskaya, O. Mashtalir, C. E. Ren, Y. Dall'Agnese, P. Rozier, P. L. Taberna, M. Naguib, P. Simon, M. W. Barsoum, and Y. Gogotsi, "Cation intercalation and high volumetric capacitance of two-dimensional titanium carbide," *Science* **341**(6153), 1502–1505 (2013).
- ¹³⁴M. Naguib, M. Kurtoglu, V. Presser, J. Lu, J. Niu, M. Heon, L. Hultman, Y. Gogotsi, and M. W. Barsoum, "Two-dimensional nanocrystals produced by exfoliation of Ti₃AlC₂," *Adv. Mater.* **23**(37), 4248–4253 (2011).
- ¹³⁵D. Sheberla, J. C. Bachman, J. S. Elias, C.-J. Sun, Y. Shao-Horn, and M. Dinca, "Conductive MOF electrodes for stable supercapacitors with high areal capacitance," *Nat. Mater.* **16**(2), 220–224 (2017).
- ¹³⁶L. Niu, T. Wu, M. Chen, L. Yang, J. Yang, Z. Wang, A. A. Kornyshev, H. Jiang, S. Bi, and G. Feng, "Conductive metal–organic frameworks for supercapacitors," *Adv. Mater.* **34**(52), 2200999 (2022).
- ¹³⁷E. H. Lahrar, A. Belhboub, P. Simon, and C. Merlet, "Ionic liquids under confinement: From systematic variations of the ion and pore sizes toward an understanding of the structure and dynamics in complex porous carbons," *ACS Appl. Mater. Interfaces* **12**(1), 1789–1798 (2020).
- ¹³⁸Y. M. Liu, C. Merlet, and B. Smit, "Carbons with regular pore geometry yield fundamental insights into supercapacitor charge storage," *ACS Cent. Sci.* **5**(11), 1813–1823 (2019).

- ¹³⁹E. Lahrar, I. Deroche, C. Matei Ghimbeu, P. Simon, and C. Merlet, "Simulations of ionic liquids confined in surface-functionalized nanoporous carbons: Implications for energy storage," *ACS Appl. Nano Mater.* **4**(4), 4007–4015 (2021).
- ¹⁴⁰J. Monk, R. Singh, and F. R. Hung, "Effects of pore size and pore loading on the properties of ionic liquids confined inside nanoporous CMK-3 carbon materials," *J. Phys. Chem. C* **115**(7), 3034–3042 (2011).
- ¹⁴¹Z. Liang, C. Zhao, W. Zhao, Y. Zhang, P. Srimuk, V. Presser, and G. Feng, "Molecular understanding of charge storage in MoS₂ supercapacitors with ionic liquids," *Energy Environ. Mater.* **4**(4), 631–637 (2021).
- ¹⁴²A. Ali, R. A. Tufa, F. Macedonio, E. Curcio, and E. Drioli, "Membrane technology in renewable-energy-driven desalination," *Renewable Sustainable Energy Rev.* **81**, 1–21 (2018).
- ¹⁴³H. T. El-Dessouky, H. M. Ettouney, and Y. Al-Roumi, "Multi-stage flash desalination: Present and future outlook," *Chem. Eng. J.* **73**(2), 173–190 (1999).
- ¹⁴⁴T. J. Welgemoed and C. F. Schutte, "Capacitive deionization technologyTM: An alternative desalination solution," *Desalination* **183**(1–3), 327–340 (2005).
- ¹⁴⁵Z. Y. Jin, X. M. Hu, T. Sun, and W. B. Zhang, "Capacitive deionization using a pulsed power supply for water treatment," *Desalin. Water Treat.* **160**, 23–31 (2019).
- ¹⁴⁶A. T. Nasrabadi and M. Foroutan, "Ion-separation and water-purification using single-walled carbon nanotube electrodes," *Desalination* **277**(1–3), 236–243 (2011).
- ¹⁴⁷S. Rikhtehgaran and A. Lohrasebi, "Water desalination by a designed nanofilter of graphene-charged carbon nanotube: A molecular dynamics study," *Desalination* **365**, 176–181 (2015).
- ¹⁴⁸Y. F. Mao, T. H. Zhou, L. Q. Xu, W. D. Wu, R. Wang, Z. B. Xiong, D. L. Wu, and H. C. Shi, "Molecular understanding of aqueous electrolyte properties and dielectric effect in a CDI system," *Chem. Eng. J.* **435**, 134750 (2022).
- ¹⁴⁹M. Simoncelli, N. Ganfoud, A. Sene, M. Haefele, B. Daffos, P.-L. Taberna, M. Salanne, P. Simon, and B. Rotenberg, "Blue energy and desalination with nanoporous carbon electrodes: Capacitance from molecular simulations to continuous models," *Phys. Rev. X* **8**(2), 021024 (2018).
- ¹⁵⁰Y. F. Mao, V. R. Ardham, L. Q. Xu, P. Y. Cui, and D. L. Wu, "Insight into electrosorption behavior of monovalent ions and their selectivity in capacitive deionization: An atomic level study by molecular dynamics simulation," *Chem. Eng. J.* **415**, 128920 (2021).
- ¹⁵¹M. R. Ceron, F. Aydin, S. A. Hawks, D. I. Oyarzun, C. K. Loeb, A. Deinhart, C. Zhan, T. A. Pham, M. Stadermann, and P. G. Campbell, "Cation selectivity in capacitive deionization: Elucidating the role of pore size, electrode potential, and ion dehydration," *ACS Appl. Mater. Interfaces* **12**(38), 42644–42652 (2020).
- ¹⁵²S. Bi, Y. Zhang, L. Cervini, T. Mo, J. M. Griffin, V. Presser, and G. Feng, "Permselective ion electrosorption of subnanometer pores at high molar strength enables capacitive deionization of saline water," *Sustainable Energy Fuels* **4**(3), 1285–1295 (2020).
- ¹⁵³Y. Zhang, C. Prehal, H. L. Jiang, Y. Liu, G. Feng, and V. Presser, "Ionophobicity of carbon sub-nanometer pores enables efficient desalination at high salinity," *Cell Rep. Phys. Sci.* **3**(1), 100689 (2022).
- ¹⁵⁴T. Mo, Z. Wang, L. Zeng, M. Chen, A. A. Kornyshev, M. Zhang, Y. Zhao, and G. Feng, "Energy storage mechanism in supercapacitors with porous graphdiynes: Effects of pore topology and electrode metallicity," *Adv. Mater.* **35**, e2301118 (2023).
- ¹⁵⁵T. Mo, J. Peng, W. Dai, M. Chen, V. Presser, and G. Feng, "Horn-like pore entrance boosts charging dynamics and charge storage of nanoporous supercapacitors," *ACS Nano* **17**, 14974 (2023).
- ¹⁵⁶C. Zhan, F. Aydin, E. Schwegler, A. Noy, and T. A. Pham, "Understanding cation selectivity in carbon nanopores with hybrid first-principles/continuum simulations: Implications for water desalination and separation technologies," *ACS Appl. Nano Mater.* **3**(10), 9740–9748 (2020).
- ¹⁵⁷C. Prehal, C. Koczwara, H. Amenitsch, V. Presser, and O. Paris, "Salt concentration and charging velocity determine ion charge storage mechanism in nanoporous supercapacitors," *Nat. Commun.* **9**(1), 4145 (2018).
- ¹⁵⁸M. Fichtner, K. Edström, E. Ayerbe, M. Berecibar, A. Bhowmik, I. E. Castelli, S. Clark, R. Dominko, M. Erakca, A. A. Franco, A. Grimaud, B. Horstmann, A. Latz, H. Lorrmann, M. Meeus, R. Narayan, F. Pammer, J. Ruhland, H. Stein, T. Vegge, and M. Weil, "Rechargeable batteries of the future—the state of the art from a BATTERY 2030+ perspective," *Adv. Energy Mater.* **12**(17), 2102904 (2022).
- ¹⁵⁹X. Yu and A. Manthiram, "Electrode–electrolyte interfaces in lithium-based batteries," *Energy Environ. Sci.* **11**(3), 527–543 (2018).
- ¹⁶⁰K. Xu, "Interfaces and interphases in batteries," *J. Power Sources* **559**, 232652 (2023).
- ¹⁶¹A. M. Tripathi, W.-N. Su, and B. Hwang, "In situ analytical techniques for battery interface analysis," *Chem. Soc. Rev.* **47**(3), 736–851 (2018).
- ¹⁶²Y. Wang, T. Wang, D. Dong, J. Xie, Y. Guan, Y. Huang, J. Fan, and Y.-C. Lu, "Enabling high-energy-density aqueous batteries with hydrogen bond-anchored electrolytes," *Matter* **5**(1), 162–179 (2022).
- ¹⁶³P. Li, Y. Jiang, Y. Hu, Y. Men, Y. Liu, W. Cai, and S. Chen, "Hydrogen bond network connectivity in the electric double layer dominates the kinetic pH effect in hydrogen electrocatalysis on Pt," *Nat. Catal.* **5**(10), 900–911 (2022).
- ¹⁶⁴A. H. Shah, Z. Zhang, Z. Huang, S. Wang, G. Zhong, C. Wan, A. N. Alexandrova, Y. Huang, and X. Duan, "The role of alkali metal cations and platinum-surface hydroxyl in the alkaline hydrogen evolution reaction," *Nat. Catal.* **5**(10), 923–933 (2022).
- ¹⁶⁵L. Ma, T. P. Pollard, Y. Zhang, M. A. Schroeder, M. S. Ding, A. V. Cresce, R. Sun, D. R. Baker, B. A. Helms, E. J. Maginn, C. Wang, O. Borodin, and K. Xu, "Functionalized phosphonium cations enable zinc metal reversibility in aqueous electrolytes," *Angew. Chem.* **133**(22), 12546 (2021).
- ¹⁶⁶N. Yao, X. Chen, Z.-H. Fu, and Q. Zhang, "Applying classical, *ab initio*, and machine-learning molecular dynamics simulations to the liquid electrolyte for rechargeable batteries," *Chem. Rev.* **122**(12), 10970–11021 (2022).
- ¹⁶⁷J. B. Goodenough and K.-S. Park, "The Li-ion rechargeable battery: A perspective," *J. Am. Chem. Soc.* **135**(4), 1167–1176 (2013).
- ¹⁶⁸J. Vatamanu, O. Borodin, and G. D. Smith, "Molecular dynamics simulation studies of the structure of a mixed carbonate/LiPF₆ electrolyte near graphite surface as a function of electrode potential," *J. Phys. Chem. C* **116**(1), 1114–1121 (2012).
- ¹⁶⁹L. Yu, H. Liu, Y. Wang, N. Kuwata, M. Osawa, J. Kawamura, and S. Ye, "Preferential adsorption of solvents on the cathode surface of lithium ion batteries," *Angew. Chem. Int. Ed.* **52**(22), 5753–5756 (2013).
- ¹⁷⁰O. Borodin, X. Ren, J. Vatamanu, A. von Wald Cresce, J. Knap, and K. Xu, "Modeling insight into battery electrolyte electrochemical stability and interfacial structure," *Acc. Chem. Res.* **50**(12), 2886–2894 (2017).
- ¹⁷¹D. W. McOwen, D. M. Seo, O. Borodin, J. Vatamanu, P. D. Boyle, and W. A. Henderson, "Concentrated electrolytes: Decoding electrolyte properties and reassessing Al corrosion mechanisms," *Energy Environ. Sci.* **7**(1), 416–426 (2014).
- ¹⁷²J. Shin and J. W. Choi, "Opportunities and reality of aqueous rechargeable batteries," *Adv. Energy Mater.* **10**(28), 2001386 (2020).
- ¹⁷³L. Suo, O. Borodin, T. Gao, M. Olgun, J. Ho, X. Fan, C. Luo, C. Wang, and K. Xu, "Water-in-salt electrolyte enables high-voltage aqueous lithium-ion chemistries," *Science* **350**(6263), 938 (2015).
- ¹⁷⁴T. Lv and L. Suo, "Water-in-salt widens the electrochemical stability window: Thermodynamic and kinetic factors," *Curr. Opin. Electrochem.* **29**, 100818 (2021).
- ¹⁷⁵Y. Sui and X. Ji, "Anticatalytic strategies to suppress water electrolysis in aqueous batteries," *Chem. Rev.* **121**(11), 6654–6695 (2021).
- ¹⁷⁶J. Vatamanu and O. Borodin, "Ramifications of water-in-salt interfacial structure at charged electrodes for electrolyte electrochemical stability," *J. Phys. Chem. Lett.* **8**(18), 4362–4367 (2017).
- ¹⁷⁷L. Chen, J. Zhang, Q. Li, J. Vatamanu, X. Ji, T. P. Pollard, C. Cui, S. Hou, J. Chen, C. Yang, L. Ma, M. S. Ding, M. Garaga, S. Greenbaum, H.-S. Lee, O. Borodin, K. Xu, and C. Wang, "A 63 m superconcentrated aqueous electrolyte for high-energy Li-ion batteries," *ACS Energy Lett.* **5**(3), 968–974 (2020).
- ¹⁷⁸Y. Zhou, M. Su, X. Yu, Y. Zhang, J.-G. Wang, X. Ren, R. Cao, W. Xu, D. R. Baer, Y. Du, O. Borodin, Y. Wang, X.-L. Wang, K. Xu, Z. Xu, C. Wang, and Z. Zhu, "Real-time mass spectrometric characterization of the solid–electrolyte interphase of a lithium-ion battery," *Nat. Nanotechnol.* **15**(3), 224–230 (2020).
- ¹⁷⁹W. Sun, F. Wang, B. Zhang, M. Zhang, V. Küpers, X. Ji, C. Theile, P. Bicker, K. Xu, C. Wang, and M. Winter, "A rechargeable zinc-air battery based on zinc peroxide chemistry," *Science* **371**(6524), 46–51 (2021).

- ¹⁸⁰A. Zhou, J. Zhang, M. Chen, J. Yue, T. Lv, B. Liu, X. Zhu, K. Qin, G. Feng, and L. Suo, "An electric-field-reinforced hydrophobic cationic sieve lowers the concentration threshold of water-in-salt electrolytes," *Adv. Mater.* **34**(47), 2207040 (2022).
- ¹⁸¹W. Zhang, Y. Lu, L. Wan, P. Zhou, Y. Xia, S. Yan, X. Chen, H. Zhou, H. Dong, and K. Liu, "Engineering a passivating electric double layer for high performance lithium metal batteries," *Nat. Commun.* **13**(1), 2029 (2022).
- ¹⁸²H. Wang, J. Zhang, H. Zhang, W. Li, M. Chen, Q. Guo, K. C. Lau, L. Zeng, G. Feng, D. Zhai, and F. Kang, "Regulating interfacial structure enables high-voltage dilute ether electrolytes," *Cell Rep. Phys. Sci.* **3**(6), 100919 (2022).
- ¹⁸³X.-Q. Zhang, X. Chen, L.-P. Hou, B.-Q. Li, X.-B. Cheng, J.-Q. Huang, and Q. Zhang, "Regulating anions in the solvation sheath of lithium ions for stable lithium metal batteries," *ACS Energy Lett.* **4**(2), 411–416 (2019).
- ¹⁸⁴A. Wang, S. Kadam, H. Li, S. Shi, and Y. Qi, "Review on modeling of the anode solid electrolyte interphase (SEI) for lithium-ion batteries," *npj Comput. Mater.* **4**(1), 15 (2018).
- ¹⁸⁵K. Huang, S. Bi, B. Kurt, C. Xu, L. Wu, Z. Li, G. Feng, and X. Zhang, "Regulation of SEI formation by anion receptors to achieve ultra-stable lithium-metal batteries," *Angew. Chem., Int. Ed.* **60**(35), 19232–19240 (2021).
- ¹⁸⁶L. Cao, D. Li, T. Pollard, T. Deng, B. Zhang, C. Yang, L. Chen, J. Vatamanu, E. Hu, M. J. Hourwitz, L. Ma, M. Ding, Q. Li, S. Hou, K. Gaskell, J. T. Fourkas, X.-Q. Yang, K. Xu, O. Borodin, and C. Wang, "Fluorinated interphase enables reversible aqueous zinc battery chemistries," *Nat. Nanotechnol.* **16**(8), 902–910 (2021).
- ¹⁸⁷F. Wang, O. Borodin, M. S. Ding, M. Gobet, J. Vatamanu, X. Fan, T. Gao, N. Eidson, Y. Liang, W. Sun, S. Greenbaum, K. Xu, and C. Wang, "Hybrid aqueous/non-aqueous electrolyte for safe and high-energy Li-ion batteries," *Joule* **2**(5), 927–937 (2018).
- ¹⁸⁸X. Wang, M. Chen, S. Li, C. Zhao, W. Zhang, Z. Shen, Y. He, G. Feng, and Y. Lu, "Inhibiting dendrite growth via regulating the electrified interface for fast-charging lithium metal anode," *ACS Cent. Sci.* **7**(12), 2029–2038 (2021).
- ¹⁸⁹Q. Wu, M. T. McDowell, and Y. Qi, "Effect of the electric double layer (EDL) in multicomponent electrolyte reduction and solid electrolyte interphase (SEI) formation in lithium batteries," *J. Am. Chem. Soc.* **145**(4), 2473–2484 (2023).
- ¹⁹⁰A. C. Thenuwara, P. P. Shetty, N. Kondekar, S. E. Sandoval, K. Cavallaro, R. May, C.-T. Yang, L. E. Marbella, Y. Qi, and M. T. McDowell, "Efficient low-temperature cycling of lithium metal anodes by tailoring the solid-electrolyte interphase," *ACS Energy Lett.* **5**(7), 2411–2420 (2020).
- ¹⁹¹S. Yuvaraja, A. Nawaz, Q. Liu, D. Dubal, S. G. Surya, K. N. Salama, and P. Sonar, "Organic field-effect transistor-based flexible sensors," *Chem. Soc. Rev.* **49**(11), 3423–3460 (2020).
- ¹⁹²S. Kim, J. Nah, I. Jo, D. Shahjerdi, L. Colombo, Z. Yao, E. Tutuc, and S. K. Banerjee, "Realization of a high mobility dual-gated graphene field-effect transistor with Al₂O₃ dielectric," *Appl. Phys. Lett.* **94**(6), 062107 (2009).
- ¹⁹³M. H. Park, Y. H. Lee, H. J. Kim, Y. J. Kim, T. Moon, K. D. Kim, J. Müller, A. Kersch, U. Schroeder, T. Mikolajick, and C. S. Hwang, "Ferroelectricity and anti-ferroelectricity of doped thin HfO₂-based films," *Adv. Mater.* **27**(11), 1811–1831 (2015).
- ¹⁹⁴H. Du, X. Lin, Z. Xu, and D. Chu, "Electric double-layer transistors: A review of recent progress," *J. Mater. Sci.* **50**(17), 5641–5673 (2015).
- ¹⁹⁵U. J. Kim, T. G. Kim, Y. Shim, Y. Park, C.-W. Lee, T.-H. Kim, H. S. Lee, D.-Y. Chung, J. Kihm, Y.-G. Roh, J. Lee, H. Son, S. Kim, J. Hur, and S. W. Hwang, "Modulation of the Dirac point voltage of graphene by ion-gel dielectrics and its application to soft electronic devices," *ACS Nano* **9**(1), 602–611 (2015).
- ¹⁹⁶J. M. Black, J. Come, S. Bi, M. Zhu, W. Zhao, A. T. Wong, J. H. Noh, P. R. Pudasaini, P. Zhang, M. B. Okatan, S. Dai, S. V. Kalinin, P. D. Rack, T. Z. Ward, G. Feng, and N. Balke, "Role of electrical double layer structure in ionic liquid gated devices," *ACS Appl. Mater. Interfaces* **9**(46), 40949–40958 (2017).
- ¹⁹⁷W. Zhao, S. Bi, N. Balke, P. D. Rack, T. Z. Ward, S. V. Kalinin, S. Dai, and G. Feng, "Understanding electric double-layer gating based on ionic liquids: From nanoscale to macroscale," *ACS Appl. Mater. Interfaces* **10**(49), 43211–43218 (2018).
- ¹⁹⁸W. Zhao, S. Bi, C. Zhang, P. D. Rack, and G. Feng, "Adding solvent into ionic liquid-gated transistor: The anatomy of enhanced gating performance," *ACS Appl. Mater. Interfaces* **11**(14), 13822–13830 (2019).
- ¹⁹⁹C. Zhang, W. Zhao, S. Bi, C. M. Rouleau, J. D. Fowlkes, W. L. Boldman, G. Gu, Q. Li, G. Feng, and P. D. Rack, "Low-temperature charging dynamics of the ionic liquid and its gating effect on FeSe_{0.5}Te_{0.5} superconducting films," *ACS Appl. Mater. Interfaces* **11**(19), 17979–17986 (2019).
- ²⁰⁰N. Onofrio and A. Strachan, "Voltage equilibration for reactive atomistic simulations of electrochemical processes," *J. Chem. Phys.* **143**(5), 054109 (2015).
- ²⁰¹H. G. Lee, S. Y. Kim, and J. S. Lee, "Dynamic observation of dendrite growth on lithium metal anode during battery charging/discharging cycles," *npj Comput. Mater.* **8**(1), 103 (2022).
- ²⁰²C. Qian, Y. Wang, H. He, F. Huo, N. Wei, and S. Zhang, "Lower limit of interfacial thermal resistance across the interface between an imidazolium ionic liquid and solid surface," *J. Phys. Chem. C* **122**(38), 22194–22200 (2018).
- ²⁰³C. Qian, B. Ding, Z. Wu, W. Ding, F. Huo, H. He, N. Wei, Y. Wang, and X. Zhang, "Ultralow thermal resistance across the solid–ionic liquid interface caused by the charge-induced ordered ionic layer," *Ind. Eng. Chem. Res.* **58**(43), 20109–20115 (2019).
- ²⁰⁴Z. Fan, Y. Wang, P. Ying, K. Song, J. Wang, Y. Wang, Z. Zeng, K. Xu, E. Lindgren, J. M. Rahm, A. J. Gabourie, J. Liu, H. Dong, J. Wu, Y. Chen, Z. Zhong, J. Sun, P. Erhart, Y. Su, and A.-N. T. Cpuud, "GPUMD: A package for constructing accurate machine-learned potentials and performing highly efficient atomistic simulations," *J. Chem. Phys.* **157**(11), 114801 (2022).
- ²⁰⁵Y. Zhang, H. Wang, W. Chen, J. Zeng, L. Zhang, H. Wang, and E. Weinan, "DP-GEN: A concurrent learning platform for the generation of reliable deep learning based potential energy models," *Comput. Phys. Commun.* **253**, 107206 (2020).
- ²⁰⁶M. Salanne, J. M. Buriak, X. Chen, W. Chueh, M. C. Hersam, and R. E. Schaak, "Best practices for simulations and calculations of nanomaterials for energy applications: Avoiding "garbage in, garbage out"," *ACS Nano* **17**(7), 6147–6149 (2023).